Tree Physiology 43, 1653–1674
https://doi.org/10.1093/treephys/tpad074

Research paper

Inhibition of DNA and RNA methylation disturbs root development of moso bamboo

Yuxiang Liufu[1,†], Feihu Xi[2,†], Lin Wu[1], Zeyu Zhang[1], Huihui Wang[1], Huiyuan Wang[1], Jun Zhang[1], Baijie Wang[1], Wenjing Kou[1], Jian Gao[3], Liangzhen Zhao[2], Hangxiao Zhang[3] and Lianfeng Gu[4,5]

[1]College of Forestry, Basic Forestry and Proteomics Research Center, Fujian Agriculture and Forestry University, No. 15 Shangxiadian Road, Cangshan District, Fuzhou City, Fujian Province 350002, China; [2]College of Life Science, Fujian Agriculture and Forestry University, Fuzhou 350002, China; [3]Key Laboratory of Bamboo and Rattan Science and Technology, State Forestry Administration, International Center for Bamboo and Rattan, Beijing 100102, China; [4]Basic Forestry and Proteomics Research Center, College of Forestry, School of Future Technology, Fujian Agriculture and Forestry University, No. 15 Shangxiadian Road, Cangshan District, Fuzhou City, Fujian Province 350002, China; [5]Corresponding author (lfgu@fafu.edu.cn)

Received February 4, 2023; Accepted June 3, 2023; handling Editor Isabel Allona

DNA methylation (5mC) and N^6-methyladenosine (m^{6}A) are two important epigenetics regulators, which have a profound impact on plant growth development. *Phyllostachys edulis* (*P. edulis*) is one of the fastest spreading plants due to its well-developed root system. However, the association between 5mC and m^{6}A has seldom been reported in *P. edulis*. In particular, the connection between m^{6}A and several post-transcriptional regulators remains uncharacterized in *P. edulis*. Here, our morphological and electron microscope observations showed the phenotype of increased lateral root under RNA methylation inhibitor (DZnepA) and DNA methylation inhibitor (5-azaC) treatment. RNA epitranscriptome based on Nanopore direct RNA sequencing revealed that DZnepA treatment exhibits significantly decreased m^{6}A level in the 3′-untranslated region (3′-UTR), which was accompanied by increased gene expression, full-length ratio, higher proximal poly(A) site usage and shorter poly(A) tail length. DNA methylation levels of CG and CHG were reduced in both coding sequencing and transposable element upon 5-azaC treatment. Cell wall synthesis was impaired under methylation inhibition. In particular, differentially expressed genes showed a high percentage of overlap between DZnepA and 5-azaC treatment, which suggested a potential correlation between two methylations. This study provides preliminary information for a better understanding of the link between m^{6}A and 5mC in root development of moso bamboo.

Keywords: alternative polyadenylation, DNA methylation, long non-coding RNA, N^6-methyladenosine, *Phyllostachys edulis*, poly(A) tail length.

Introduction

DNA and RNA methylations regulate complicated gene expression of organisms without alteration of the DNA sequence (Rapp and Wendel 2005, Gallusci et al. 2017). More than 170 RNA modifications have been reported (Wiener and Schwartz 2021). Among these chemically modified RNA residues, N^6-methyladenosine (m^{6}A) is one of the most prevalent RNA methylation in eukaryotes (Arribas-Hernández and Brodersen 2020). In recent years, RNA modification has been an emerging research hotspot because addition and removal of N^6-methyl groups from adenine is a dynamic and reversible biological process due to methyltransferases and demethylases (Jia et al. 2011). In mammals, the addition of m^{6}A is mediated by the methyltransferase complex, such as METTL3 and METTL14 (Liu et al. 2014). In *Arabidopsis thaliana*, m^{6}A writer components include MTA, MTB, FIP37, VIRILIZER and HAKAI (Zhong et al. 2008, Shen et al. 2016, Růžička et al. 2017). Demethylase activity is observed in Fat mass and obesity associated gene (FTO) and alpha-ketoglutarate-dependent dioxygenase homolog (ALKBH) family, which are responsible for the removal

[†]These authors contributed equally to this manuscript.

of m^{6}A in mammals and *Arabidopsis*, respectively (Jia et al. 2011, Zheng et al. 2013, Duan et al. 2017). In addition, m^{6}A binding proteins containing YTH domain specifically recognize the adenosine with N^6-methyl group on the conserved motifs and ultimately perform specific biological functions (Theler et al. 2014).

The distribution of m^{6}A is predominantly enriched in the terminal coding regions or 3′-UTR (Luo et al. 2014, Miao et al. 2020). Multiple studies give insight into the regulation of m^{6}A, including mRNA stability (Wei et al. 2018, Lee et al. 2020, Guo et al. 2022), nuclear-cytoplasmic localization (Roundtree et al. 2017, Edens et al. 2019), alternative polyadenylation site (Yue et al. 2018, Song et al. 2021), poly(A) tail length (Parker et al. 2020) and translation efficiency (Coots et al. 2017). In plants, genetic evidence established the influence of m^{6}A on trichome morphology and leaf formation (Arribas-Hernández et al. 2018), flower transition (Duan et al. 2017), circadian rhythm (Fustin et al. 2013, Zhong et al. 2018), biomass and fruit ripening (Zhou et al. 2019, Yu et al. 2021, Hu et al. 2022), anther development (Ma et al. 2021), and stress response (Lu et al. 2020, Zhu et al. 2021). The S-adenosylhomocysteine hydrolase inhibitor 3-Deazaneplanocin A (DZnepA) is known as an m^{6}A methylators inhibitor through decreasing activity of S-adenosylmethionine-dependent methyltransferase (Glazer et al. 1986, Fustin et al. 2013). DZnepA-based hypomethylation of m^{6}A plays crucial roles in circadian rhythm in mammals (Fustin et al. 2013, Zhong et al. 2018), acceleration of fruit ripening in tomato (Hu et al. 2022) and repression of the synthesis of the genome in severe acute respiratory syndrome coronavirus 2 (Kumar et al. 2022).

In addition to RNA methylation, DNA methylators is also regulated by methylating and demethylating enzymes, which has an important role in genome stability and gene regulation in plant (Zhang et al. 2018). The maintenance of 5mC is catalyzed by different DNA methyltransferases. For instance, methyltransferase 1 (MET1) is mainly responsible for the methyl addition of the CG context, while CHG methylators is maintained by DNA methyltransferase chromomethylase 3 (CMT3) and chromomethylase 2 (CMT2) (Bartee et al. 2001, Kankel et al. 2003, Stroud et al. 2014). CHH (H = A, T or C) motif is context-independent and predominantly mediated by the RNA-directed DNA methylators pathway (RdDM), which is methylated by DRM2 (Jones et al. 2001, Naumann et al. 2011). The families of *SUVH* and *AGO* play important roles in the pathways of RdDM (Jackson et al. 2002, 2004, Malagnac et al. 2002). In *Arabidopsis*, mutation of the H3K9-specific methyltransferase *SUVH* reduces CHG methylators levels (Ebbs and Bender 2006). Similar to the regulation of RNA methylation, DNA methylators is dynamically reversible, which is regulated by subfamilies of bifunctional DNA glycosylases to remove methylcytosines from 5mC (Penterman et al. 2007, Law and Jacobsen 2010). In *Arabidopsis*, there are four bifunctional 5mC DNA glycosylase families, including repressor of silencing 1 (ROS1) (Zhu et al. 2007), DEMETER (DME) (Schoft et al. 2011), Demeter-like protein 2 (DML2) and DML3, which recognize all sequence contexts cytosine for removal of 5-methylcytosines (Ortega-Galisteo et al. 2008). DNA methylators plays crucial roles in regulation of gene expression, transposon silencing and maintenance of genome stability (Kumar and Mohapatra 2021). It also plays essential functions in fruit ripening (Zhong et al. 2013, Daccord et al. 2017, Zhou et al. 2019), seed development (Grover et al. 2018), embryo-to-seedling transition (Bouyer et al. 2017), regeneration of shoots (Shemer et al. 2015) and heat stress response in roots (Hossain et al. 2017). The 5-azacytidine (5-azaC) acts as inhibitor of DNA methyltransferase through suppressing the activity of DNA methyltransferase (Friedman 1979, Christman 2002). The 5-azaC-mediated hypomethylation leads to an earlier flowering in *Arabidopsis* (Burn et al. 1993), the improvement of salt resistance in *Triticum aestivum* L. (Zhong et al. 2010), and an increase in tanshinone biosynthesis on hairy roots of *Salvia miltiorrhiza* (Yang et al. 2022).

It is essential to identify RNA and DNA modifications using well-developed technology. Oxford Nanopore Technology (ONT) long-read sequencing has now emerged as a novel technique for identifying nucleotide modifications, based on differences between modified and unmodified bases (Rand et al. 2017, Simpson et al. 2017, Liu et al. 2019). Since ONT sequencing is based on the current signal to distinguish features of a base and its modification, it has gradually become a reliable technology for identifying both RNA and DNA modifications at single-nucleotide resolution (Garalde et al. 2018, Smith et al. 2019, Jenjaroenpun et al. 2021). However, whole-genome bisulfite sequencing (BS-seq) is still the gold standard technique for identification of DNA methylators due to high resolution and accuracy (Plongthongkum et al. 2014).

In addition to identification of methylation, ONT also can identify alternative polyadenylation (APA) and poly(A) tail length (PAL) (Gao et al. 2022, Li et al. 2022, Zhou et al. 2022). Alternative polyadenylation plays important roles in biological development and response to environmental stress (Li et al. 2017*b*, Xu et al. 2022). Alternative polyadenylation events generate different isoforms with variable 3′-untranslated region (3′-UTR) lengths, which is subject to complex regulation (Shen et al. 2011, MacDonald 2019). For example, *CPSF30* in *Arabidopsis* constitutes the core component of the CPSF complex, regulating the selection of polyadenylation sites (Thomas et al. 2012, Li et al. 2017). It is extremely critical to identify APA position for quantification. Direct RNA sequencing (DRS) based on poly(A) tail capturing has a natural advantage in the detection of APA (Garalde et al. 2018). Theoretically, the position of the 3′-UTR end of each DRS read symbolizes potential polyadenylation site (Parker et al. 2020). In addition to APA, the poly(A) tail plays essential roles in maintaining mRNA stability, improving

translation efficiency and cytoplasmic localization (Passmore and Coller 2022). Poly(A) polymerase and deadenylase dynamically regulate PAL (Goldstrohm and Wickens 2008, Nicholson and Pasquinelli 2019). The nanopore-based method could provide a comprehensive profile of PAL in plants (J. Jia et al. 2022).

Phyllostachys edulis (*P. edulis*), a bamboo species of the subfamily Poaceae, occupies an important position in the forestry economy and industrial structure due to huge economic benefits in the utilization of wood and shoots (Chaowana 2013, Peng et al. 2013). *Phyllostachys edulis* presents an obvious biological characteristic of rapid growth during bamboo shoot state due to the expansion of underground rhizome–root system (Li et al. 2000, 2018, Song et al. 2016). Although epigenetic studies have been reported in a variety of woody plants (Hu et al. 2020, Lu et al. 2020, Hou et al. 2022, Li et al. 2022), the association between methylators and root development remains unexplored in *P. edulis*. In this study, we selected root with DZnepA and 5-azaC treatment as materials to investigate the correlations between reduced methylators and root development in *P. edulis*. In particular, this study provides preliminary clues about the association between RNA methylators and DNA methylators to promote investigation of potential interplay in future.

Materials and methods

Moso bamboo material inhibitor treatment and growing environment

Phyllostachys edulis seeds were soaked in sterile water overnight and then surface-sterilized with chlorine gas. We planted disinfected seed in 2-ml centrifuge tubes containing 1 ml of MS medium to avoid bacteria pollution. Then, the seeds were germinated at 26 °C for 8–9 days under dark conditions. Finally, the sterile seedlings were planted and cultured in MS plates containing different concentrations of DZnepA and 5-azaC for 2 weeks in a constant temperature tissue culture room at 26 °C and under long-day light conditions (16L/8D).

Construction of RNA-seq library and bioinformatics analysis of short reads

In this study, we constructed dUTP strand-specific libraries. Briefly, fragments of ~400–500 nt in length were excised from a 2% agarose gel and the dUTP libraries were constructed and sequenced using the Illumina HiSeq 2500 platform to generate paired sequences of 125 nt in length. We used hisat2 (Kim et al. 2019) to map short reads to reference genome of *P. edulis* with following parameters: –wrapper basic-0 –max-intronlen 20,000 –dta. Then, we used samtools (Li et al. 2009) to convert and sort the bam file. The original expression matrix was identified by featureCounts (Liao et al. 2014) based on sorted bam files. The false discovery rate (FDR) was determined using EdgeR (Robinson et al. 2010) based on the count of raw reads. The gene expression was normalized by transcripts per million (TPM). Then, differentially expressed genes (DEGs) were identified based on log2 fold-change cutoffs of 1.5 and FDR < 0.05.

Construction of DRS libraries and bioinformatics analysis of DRS long reads

Total RNAs were extracted from fresh samples according to the protocol RNA extraction kit (TIANGEN, Cat.no DP441, Beijing, China). Deoxyribonuclease I was used for removal of DNA from RNA. The RNA quality was detected by agarose gel electrophoresis. Total RNAs from different samples were quantified by Qubit RNA HS Assay Kit (ThermoFisher, Cat. No. Q32855, USA). The purity of total RNAs was determined by Nanodrop 2000c spectrophotometer. The RNA integrity number (RIN) value of total RNA samples was determined by 2100 Bioanalyzer and RNA 6000 Nano Kit (Agilent, Cat. No. 5067-1511, CA, USA). The samples with RIN value >8 were used for DRS libraries. The enrichment of mRNA was performed by Dynabeads™ mRNA Purification Kit (Invitrogen, Cat. No. 61006, USA). The poly(A) + RNAs was ligated to the ONT reverse transcription adapter (RTA) based on oligo d(A). After the first strand of cDNA was obtained using reverse transcription PCR, the sequencing adapter was ligated to initiate sequencing using SQK-RNA002 kit protocol with MinION device and R9.4.1 flow cell (FLO-MIN106, Oxford, UK).

We used Guppy v3.6.1 for converting DRS raw current signals based on ONT platform into FASTQ files, which were further corrected by LoRDEC (Salmela and Rivals 2014) with the parameter (-k 19 -s 3) using RNA-seq reads based on the Illumina platform. The corrected long reads were then mapped onto bamboo genome (Zhao et al. 2018) using minimap2 (Li 2018) by the command (minimap2 -ax splice -uf -k14 –sam-hit-only –secondary = no). Alignment files were sorted, indexed and filtered (-F 2048) by samtools. Long reads corresponding to each gene were calculated using featureCounts (Liao et al. 2014). The distance (<20 nt) between annotated translation start sites and the initial mapping site of DRS long reads was considered a standard for classification of full length reads and non-full length reads. The differential full-length ratios among pair-wise comparison (DMSO vs DZnepA and DMSO vs 5-azaC) were tested by Fisher test using the number of full-length reads and the number of non-full-length reads from two samples. $P < 0.005$ were selected as the cutoff of differential full-length ratios.

Identification of differential m^{6}A site, APA and PAL

We identified m^{6}A sites based our previous published protocol (Liufu et al. 2022). Briefly, each fast5 file was transferred into fast5 files containing only a single sequence by multi_to_single_fast5 (https://github.com/nanoporetech/ont_fast5_api). We then assigned raw signal and associated base calls to bamboo transcriptome reference sequences using the resquiggle algorithm from Tombo (Stoiber et al. 2017). Finally,

we identified and quantified m^{6}A at single-base resolution using nanom^{6}A (Gao et al. 2021). We set 20 as cutoff for the minimum number of DRS reads from DZnepA treatment supporting a modified m^{6}A site in genomic coordinates. Considering different DRS depths from different libraries, we calculated this cutoff of other libraries (DMSO and 5-azaC) according to normalization of DRS reads depth. Differential m^{6}A sites were calculated based on T test for DMSO vs DZnepA and DMSO vs5-azaC using the modification rate of each m^{6}A site. Differential m^{6}A site was identified using cutoff of $P < 0.05$ and difference log2 fold change >0.5.

Poly(A) site with >5% usage rate remained as candidate poly(A) site. The distance between two distinct poly(A) sites should be >30 nt. The reads with termination site located 12 nt immediately upstream and downstream of a poly(A) site was assigned to the poly(A) site. The poly(A) site with higher abundance was selected as the major site. The abundance for each poly(A) site was normalized based on read count from the highest sites and library size.

The QC result and PAL of each DRS read were calculated by Nanopolish (Workman et al. 2019) with default parameter. The median of PALs from all long reads was calculated for each gene. Differential gene PAL was considered as *P*-value <0.05 and log2 fold change >0.5 between DMSO and inhibitor treatment.

Identification of lncRNA

For lncRNA identification, DRS long reads were merged together and aligned to genome by minimap2 (Li 2018) to generate BAM files, which were assembled to the transcripts by Stringtie2 (Kovaka et al. 2019). Transcripts with exon lengths of <200 bp were filtered out from downstream analysis. Potential lncRNAs was selected from the overlapped candidates from three lncRNAs prediction methods (PLEK, CPC2 and lncFinder) with default options (Li et al. 2014, Kang et al. 2017, Han et al. 2019). Finally, Pfam-scan was used to calculate coding potentiality based on protein family domains (*E*-value < e-5) to further discard potential coding transcripts (Mistry et al. 2021). Finally, non-coding transcripts expressed in at least one sample were considered as lncRNA. The identification of full-length lncRNA was calculated using distance (<20 nt) between annotated transcript start sites and the initial mapping site of DRS long reads.

DNA extraction and methylators analysis

Genomic DNA (gDNA) was extracted using a genomic DNA extraction kit (TIANGEN, Cat. No. DP305, Beijing, China). Agarose gel electrophoresis was used to detect undegraded, and then the Qubit dsDNA HS assay kit was used for accurate quantification. Finally, the gDNA was determined OD260/280 was about 1.80, and OD260/230 was about 2.0–2.2 through Nanodrop 2000c UV spectrophotometer (ThermoFisher, Cat. No. 11840461, USA). The gDNA that has passed the standard was used for downstream bisulfite sequencing library construction.

We used the bismark_genome_preparation command of the bismark (Krueger and Andrews 2011) software to index the *P. edulis* genome. Furthermore, we used the bismark_methylation_extractor command with the parameters -p –no_overlap –comprehensive –report –bedGraph –CX_report –scaffolds –cytosine_report to obtain DNA 5mC methylators information from CX report file.

GO enrichment analysis

The annotated genes were downloaded from bambooGDB database (Zhao et al. 2014) and annotated with BLAST2GO (Conesa et al. 2005) to construct the bamboo Gene Ontology (GO) database. Gene Ontology enrichment analysis of differential genes was performed using clusterProfiler (Yu et al. 2012), and the Benjamini and Hochberg test was used to verify the enrichment results (GO terms) with FDR < 0.05.

Results

Methylation inhibitors generated obvious phenotype on root development

In this study, we used methylators inhibitors as treatment and DMSO as control to investigate the effect of methylators on root development in *P. edulis* (Figure 1A). Among six concentration gradient of methylators inhibitors, shorter root length was observed in response to high concentrations of DZnepA (Figure 1B) and 5-azaC (Figure 1C). Moreover, treatment with methylators inhibitors increased lateral root density and the elongation of the main root was completely inhibited at 10 μM concentrations for both DZnepA and 5-azaC (Figure 1D). Root apical meristem shown gradually decreased cell density under treatment of 5-azaC and DZnepA (Figure S1 available as Supplementary data at *Tree Physiology* Online). Furthermore, paraffin wax sections following light microscopical examination among eight consecutive time points (Days 0–7) revealed that the lateral root primordial cell differentiation event happened at Day 4 using 10 μM concentrations for two inhibitors (Figure 1E). Day 3 was the key time point when the lateral root primordium cells were ready to differentiate. Thus, we collected the root tip materials with 10 μM 5-azaC and DZnepA treatment on Day 3 to explore the role of 5mC and m^{6}A methylators in root development of *P. edulis*.

DZnepA treatment generated global hypomethylated m^{6}A in 3′-UTR region

To evaluate the dynamics of the epitranscriptome in response to two methylators inhibitors, we used both MinION sequencer and Illumina RNA-seq reads for transcriptome sequencing using total RNAs from root tips treated by DMSO, DZnepA and 5-azaC, respectively (Figure 1A). A total of about 10 million DRS

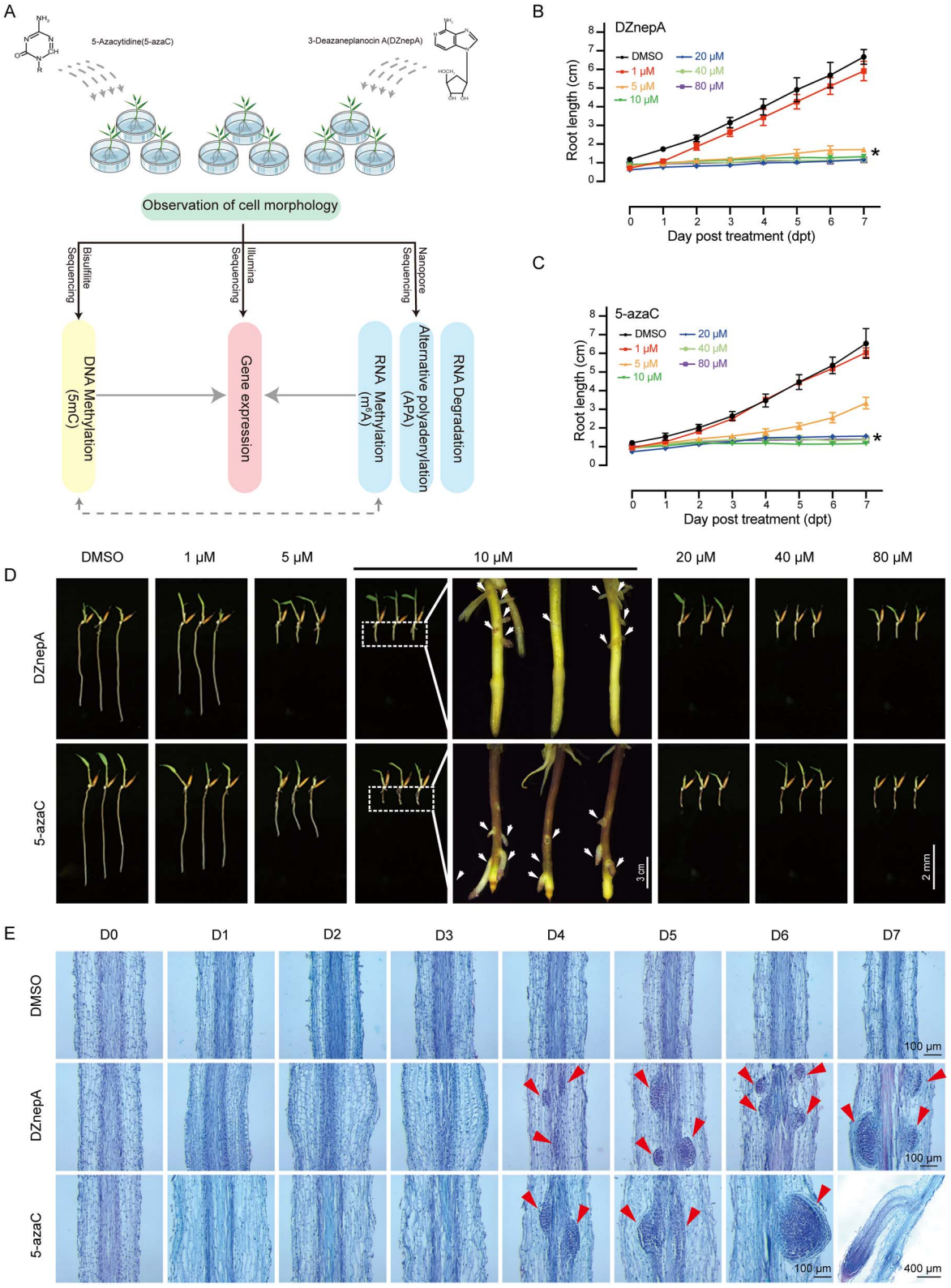

Figure 1. Phenotype and cell morphology of moso bamboo root upon inhibitors treatment. (A) Flowchart for analysis of methylators changes in root induced by DZnepA and 5-azaC. (B) Curve of root growth under treatment of different concentrations of DZnepA. (C) Curve of root growth under treatment of different concentrations of 5-azaC. (D) Phenotype of moso bamboo under treatment of different concentrations of DZnepA and 5-azaC. (E) Cytological effects of moso bamboo roots under 0–7 days of treatment by DZnepA and 5-azaC.

long reads were generated. The average alignment rate to the annotation files and reference genome was 86.03 and 94.31%, respectively (Table S1 available as Supplementary data at *Tree Physiology* Online), which suggested that DRS reads in this study covered most of the annotated genes. Then, we performed nanom6A (Gao et al. 2021) based on these DRS reads to quantitatively detect m^{6}A modification at the single-base resolution. We identified a total of 65,912, 61,696 and 49,197 m^{6}A sites associated with 13,131, 12,029 and 12,172 genes in DMSO, DZnepA and 5-azaC samples, respectively (Figure S2 available as Supplementary data at *Tree Physiology* Online). Gene Ontology (GO) analysis shown that genes with common m^{6}A modification were enriched in ligase activity, GTPase activity, mRNA binding and protein translation genes (Figure S3 and Table S2 available as Supplementary data at *Tree Physiology* Online). The distribution of m^{6}A sites was dominantly enriched around the end of the coding sequencing (CDS) and 3′-UTR (Figure 2A). The percentage of m^{6}A in different regions was slightly different in DZnepA and 5-azaC by comparison with DMSO (Figure 2B). As expected, we observed significantly decreased m^{6}A ratio after DZnepA treatment (Kolmogorov–Smirnov test) (Figure 2C). However, we did not observe obvious global change of m^{6}A ratio upon 5-azaC treatment (Figure 2C, left panel). The expression levels of two *PedMTAs* (PH02Gene01512 and PH02Gene03311) increased upon DZnepA treatment (Table S3 available as Supplementary data at *Tree Physiology* Online), which were further validated by qPCR (Figure 2C, right panel). The increased expression of m^{6}A writers might partly antagonize the hypomethylated m^{6}A upon RNA inhibitor treatment.

In total, we identified 7416 genes with decreasing m^{6}A ratio and 2824 genes with increasing m^{6}A ratio upon DZnepA treatment (Figure S4 available as Supplementary data at *Tree Physiology* Online). Furthermore, we identified differential m^{6}A sites upon inhibitor treatment using cut-off of *P*-value <0.05 (Fisher's exact test) and log2 fold change (m^{6}A ratio upon DZnepA treatment/m^{6}A ratio upon DMSO treatment) greater or less than 0.5 or −0.5, respectively. Among these sites, we identified 121 hypermethylated and 6548 hypomethylated sites (left panel in Figure 2D; Table S4 available as Supplementary data at *Tree Physiology* Online), which further demonstrated global reductions of m^{6}A ratio upon DZnepA treatment. AAACA and AAACT were two most common motifs among hypomethylation sites (right panel, Figure 2D). For 5-azaC treatment, we did not observe large proportion of differences in modification sites. In total, there were 346 hypermethylation sites and 171 hypomethylation sites (left panel in Figure 2E). GAACT and GGACA were two most common motifs among hypomethylation and hypermethylation sites, respectively (right panel in Figure 2E).

It was noteworthy that the distribution of hypermethylation sites and hypomethylation sites upon inhibitors treatment tended to locate in coding region (CDS) and 3′-UTR region, respectively (Figure 2F and G). For example, *MKK3* is annotated as mitogen-activated protein kinase activity, which regulates adventitious root (Bai and Matton 2018). The modification rate in the 3′-UTR of *PedMKK3* was significantly reduced under m^{6}A inhibitor treatment ($P < 0.005$, Fisher's exact test) (Figure 2H). However, *PedMKK3* presented increased methylators in three m^{6}A sites from CDS region (Figure 2H). In addition, we observed increased methylators ratio in 4 m^{6}A sites from CDS and decreased methylators ratio in 1 m^{6}A site from 3′-UTR in *PedMTA* (PH02Gene03311) upon DZnepA treatment (Figure S5 available as Supplementary data at *Tree Physiology* Online).

The ratio of full-length reads was associated with m^{6}A level under DZnepA treatment

The stability of mRNA is related to the ratio of full-length reads and non-full-length reads in mRNA (Wang et al. 2014). Long reads from DRS sequencing can capture the complete mRNA for quantitative analysis under different treatment (Gao et al. 2022). The proportion of full-length read in DMSO, DZnepA and 5-azaC treated samples was 41.81, 50.16 and 27.75%, respectively (Figure 3A). Furthermore, we identified 2258 genes with increased full-length ratio (Figure 3B) upon DZnepA treatment, and 3102 genes with decreasing full-length ratio (Figure 3C) upon 5-azaC treatment (*P*-value <0.005, Fisher's exact test) (Table S5 available as Supplementary data at *Tree Physiology* Online). Gene Ontology analysis showed 2258 genes with increasing full-length ratios upon DZnepA treatment were enriched in the GO term of glutathione-related and gluconeogenesis (Figure S6A available as Supplementary data at *Tree Physiology* Online), and 3102 genes with decreasing full-length ratio upon 5-azaC treatment were enriched in reduction reactions, protein unfolding and degradation and carbohydrate utilization and metabolism (Figure S6B available as Supplementary data at *Tree Physiology* Online). With hypergeometric test, the two types of genes show significantly overlap between DZnepA and 5-azaC treatment (Figure 3D). The full-length ratio of the 1121 genes presented opposite change upon DZnepA and 5-azaC treatment. These genes were mainly responsible for glutathione transferase activity, reductive detoxification and translation processes (Figure S6C available as Supplementary data at *Tree Physiology* Online).

We further investigated the relationship between m^{6}A and full-length ratio. We revealed higher m^{6}A ratio in full-length reads than that of no-full-length reads in all samples (Figure 3E). The 2258 genes with increasing full-length ratio upon DZnepA treatment presented reduced m^{6}A ratio for both full-length and non-full-length reads (Figure 3F). The result indicated that part m^{6}A modifications was negatively correlated with the ratio of full-length reads, which was consistent with the previous report (Wang et al. 2014, Shen et al. 2016). However, 3102

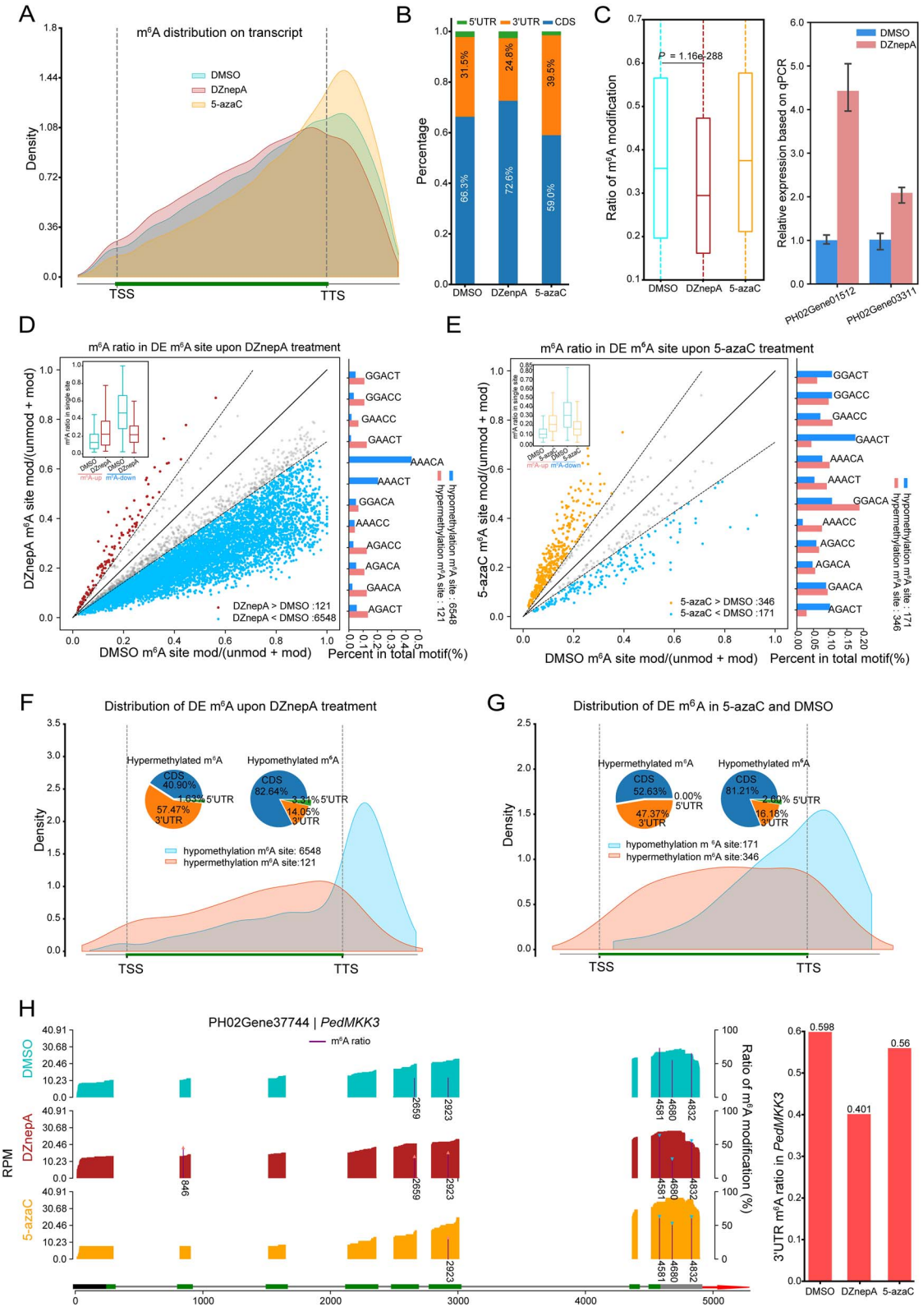

Figure 2. Profile of differential m^{6}A based on Nanopore DRS upon inhibitors treatment. (A) Distribution of m^{6}A site in UTR (gray) and CDS regions (green). (B) Histogram showing the composition of m^{6}A in CDS and UTR in DMSO, DZnepA and 5-azaC. (C) Boxplot showing the ratio distribution for m^{6}A sites in DMSO, DZnepA and 5-azaC (left panel). Validation of *PedMTAs* using qPCR (right panel). (D, E) Scatter plot showing differential m^{6}A upon DZnepA (D) and 5-azaC (E) treatment. Boxplot showing m^{6}A ratio in genes with differential methylation. Histogram on the right panel showing the motif usage of m^{6}A up-regulated and down-regulated genes. (F, G) Distribution of hypermethylation and hypomethylation m^{6}A site upon DZnepA (F) and 5-azaC (G) treatment. (H) Wiggle plot showing gene expression. Histogram showing m^{6}A ratio of *PedMKK3* in 3′-UTR.

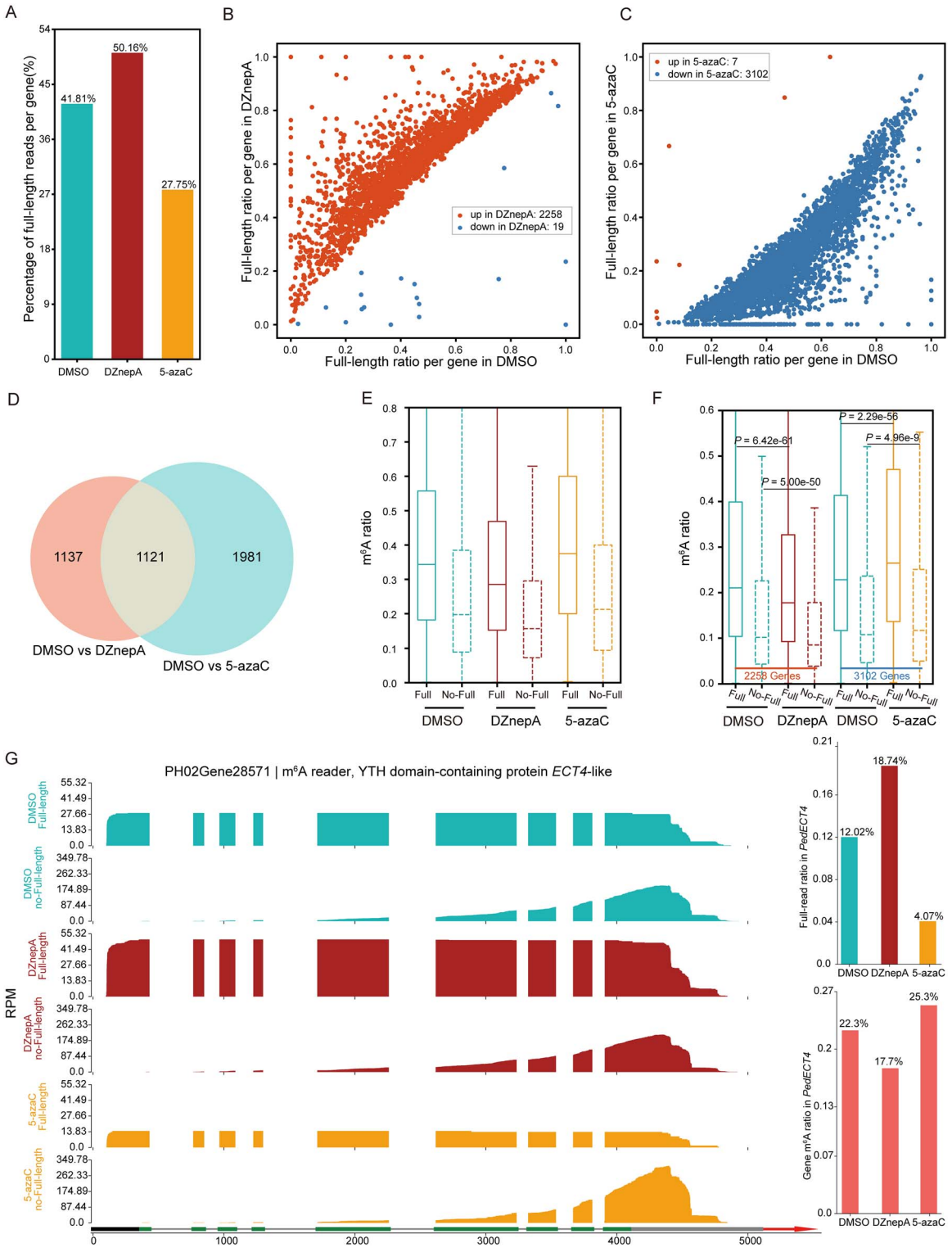

Figure 3. Overview of differential full-length ratios under inhibitors treatment. (A) Histogram showing the full-length ratio in DMSO, DZnepA and 5-azaC. (B, C) Scatter plot showing gene with increasing and decreasing full-length ratio in DZnepA (B) and 5-azaC (C), respectively. (D) Venn diagram showing overlapped genes. (E) Histogram showing m^{6}A ratio in full-length reads and no-full-length reads. (F) Histogram showing m^{6}A ratio of genes with increased full-length ratio in DZnepA and genes with decreased full-length ratio in 5-azaC. (G) Wiggle plot, showing the expression (RPM in *y*-axis) of full-length reads and non-full-length reads. Histograms in right panel presented full-length ratio and m^{6}A ratio in m^{6}A reader.

genes with decreasing full-length ratio upon 5-azaC presented increased m^{6}A ratio for both full-length and non-full-length reads (Figure 3F), which suggested the presence of potential different mechanism. YTH domain-containing protein *PedECT4* presented increased and decreased full-length ratios under treatment of DZnepA and 5-azaC, respectively (Figure 3G). However, m^{6}A ratio in 3′-UTR performed the contrary tendency (Figure 3G), suggesting that m^{6}A might promote the degradation of full-length reads.

Hypomethylated m^{6}A promotes proximal poly(A) site usage

Previous reports have demonstrated that m^{6}A plays an important part in APA and 3′-UTR formation (Xiao et al. 2016, Pontier et al. 2019, Parker et al. 2020). In this study, we characterized 16,259 genes with two or more poly(A) sites based on DRS data (Figure S7 available as Supplementary data at *Tree Physiology* Online). We further identified 1053 genes (Table S7 available as Supplementary data at *Tree Physiology* Online) that shifted to poly(A) usage upon DZnepA treatment (Fisher's exact test, *P*-value <0.05). These genes included 888 genes shifted to proximal poly(A) site and 165 genes shifted to distal poly(A) site (Figure 4A). Interestingly, we identified two m^{6}A erasers (Figure S8 available as Supplementary data at *Tree Physiology* Online) and five m^{6}A readers (Figure S9 available as Supplementary data at *Tree Physiology* Online), which presented higher PPR upon DZnepA treatment. In 5-azaC, there were 211 genes shifted to the proximal poly(A) site, while 172 genes shifted to distal poly(A) sites (Figure 4B). In addition, the genes with shift to proximal poly(A) usage had more chance to include m^{6}A sites in both DZnepA (P = 4.68e-12) and 5-azaC treatment (P = 0.007) than that of DMSO-treated control (Figure 4C), indicating that m^{6}A modification was enriched in APA shift genes. Especially, we found that genes with shift to proximal poly(A) usage have higher percentage of gene with m^{6}A than that of genes with shift to distal poly(A) usage in DZnepA (P = 0.04) (Figure 4C).

We further assessed the association between m^{6}A in 3′-UTR and PPR (proximal poly(A) site usage ratio) using above poly(A) shifted genes. Scatter plot showed most of points enriched in second quadrant (Figure 4D), which suggested that decreased m^{6}A modification in 3′-UTR was associated with APA shift to proximal poly(A) usage upon DZnepA treatment (Figure 4D). Genes with higher PPR ratio included two adagio proteins (ADO) (Krauss et al. 2009, Wang et al. 2012), SNW/SKI-interacting protein, which were responsible for regulation of circadian rhythm (Figure 4D). For example, *ClNV1* mutant exhibited inhibition of lateral root growth (Qi et al. 2007, Xiang et al. 2011). *PedClNV1* in this study presented proximal poly(A) site transition and accompanied by hypomethylated m^{6}A in 3′-UTR (Figure 4F), indicating that m^{6}A might be associated with the diversity of 3′-UTR length. However, this kind of distal-to-proximal poly(A) site shifts was not obvious upon 5-azaC treatment (Figure 4E).

Global hypomethylation shortens poly(A) tail length

Global PAL presents dynamic distribution (Roach et al. 2020, J. Jia et al. 2022). We calculated polyadenylated tail length (PAL) for each long reads using the poly(A) module from Nanopolish (Workman et al. 2019). Global PALs in DMSO-treated roots showed enrichment at 70–100 nt (Figure S10A available as Supplementary data at *Tree Physiology* Online), which were slightly longer than that in *Arabidopsis* root (J. Jia et al. 2022). The global PALs with DZnepA and 5-azaC treatment were slightly shortened compared with the DMSO treatment (Figure S10A available as Supplementary data at *Tree Physiology* Online), which indicated that methylators might be involved in PALs regulation in roots.

Previous studies propose that PAL is closely related to gene expression, m^{6}A level and mRNA half-life (Lima et al. 2017, J. Jia et al. 2022). To comprehensively ascertain the effect of PAL on expression, we firstly ranked gene expression from lowest to highest to plot corresponding PALs (Figure 5A). Increased gene expression was accompanied by progressively shorter PAL, indicating a negative correlation between gene expression and PAL (Figure 5B). Previous studies show that m^{6}A in poly(A) tail protects mRNA from degradation and RNA containing m^{6}A has a longer poly(A) tail (Viegas et al. 2022, Wu et al. 2022). Increased m^{6}A ratio was accompanied by progressively longer PAL (Figure 5C), which showed a slight positive correlation between m^{6}A and PAL (Figure 5D).

We also investigated the association between full-length ratio and PAL, which revealed a slight negative correlation between full-length ratio (Figure 5E and F). Genes with a higher proportion of full-length plausibly possessed shorter PALs, which was consistent with the idea that mRNAs with longer half-lives possessed shorter PALs (J. Jia et al. 2022). However, a similar percentage of up-regulated and down-regulated PAL was observed in genes with significant full-length ratio changing upon DZnepA (Figure S10B available as Supplementary data at *Tree Physiology* Online) and 5-azaC treatment (Figure S10C available as Supplementary data at *Tree Physiology* Online). The result implied that PAL might not be the major contributing factor in regulating full-length ratio.

We further identified significant PAL change upon inhibitor treatment (fold change > 1.5, *P*-value <0.05) (Table S8 available as Supplementary data at *Tree Physiology* Online). In total, we founded that DZnepA treatment caused 239 and 53 genes with significantly increased and decreased PAL, respectively (left panel in Figure 5G). The heatmap also presented the trend of more PAL shortening (right panel in Figure 5G). We also observed 192 genes showing PAL shortening compared with 61 genes with extending PAL in response to 5-azaC treatment (Figure 5H). Finally, we explored the effect of PAL

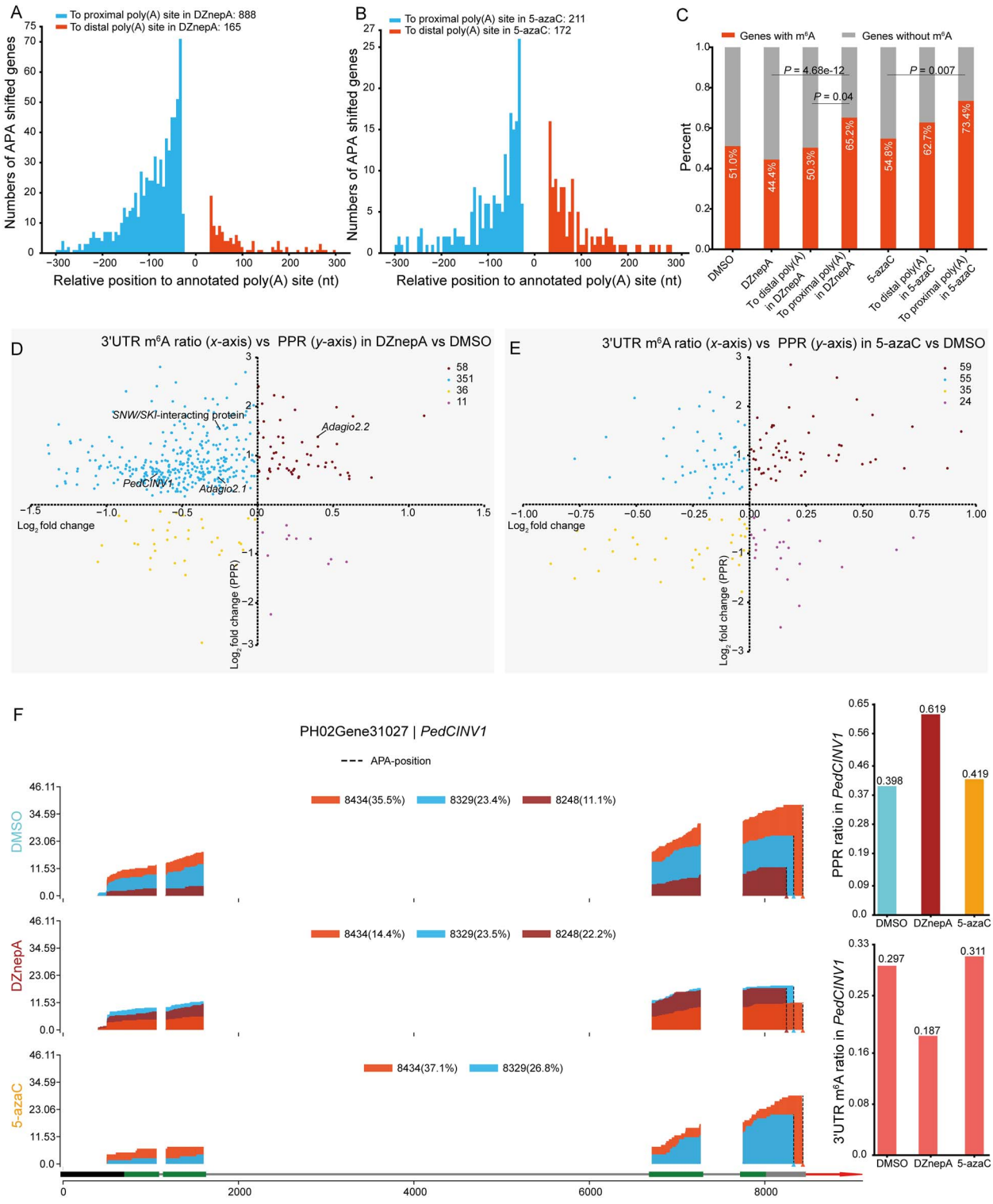

Figure 4. Dynamics of poly(A) site under methylators inhibition. (A, B) Histogram showing the distribution of proximal and distal poly(A) sites upon DZnepA (A) and 5-azaC (B) treatment. (C) Histogram showing the percentage of m^{6}A modified genes among gene with change in poly(A) usage upon DZnepA and 5-azaC treatment. (D, E) Scatter plots showing relationship between the usage of proximal poly(A) site and 3′-UTR m^{6}A ratio upon DZnepA (D) and 5-azaC (E) treatment. (F) Wiggle plot showing the alteration of poly(A) site usage. Histograms in right panel presented PPR ratio and 3′-UTR m^{6}A ratio in *PedCINV1*.

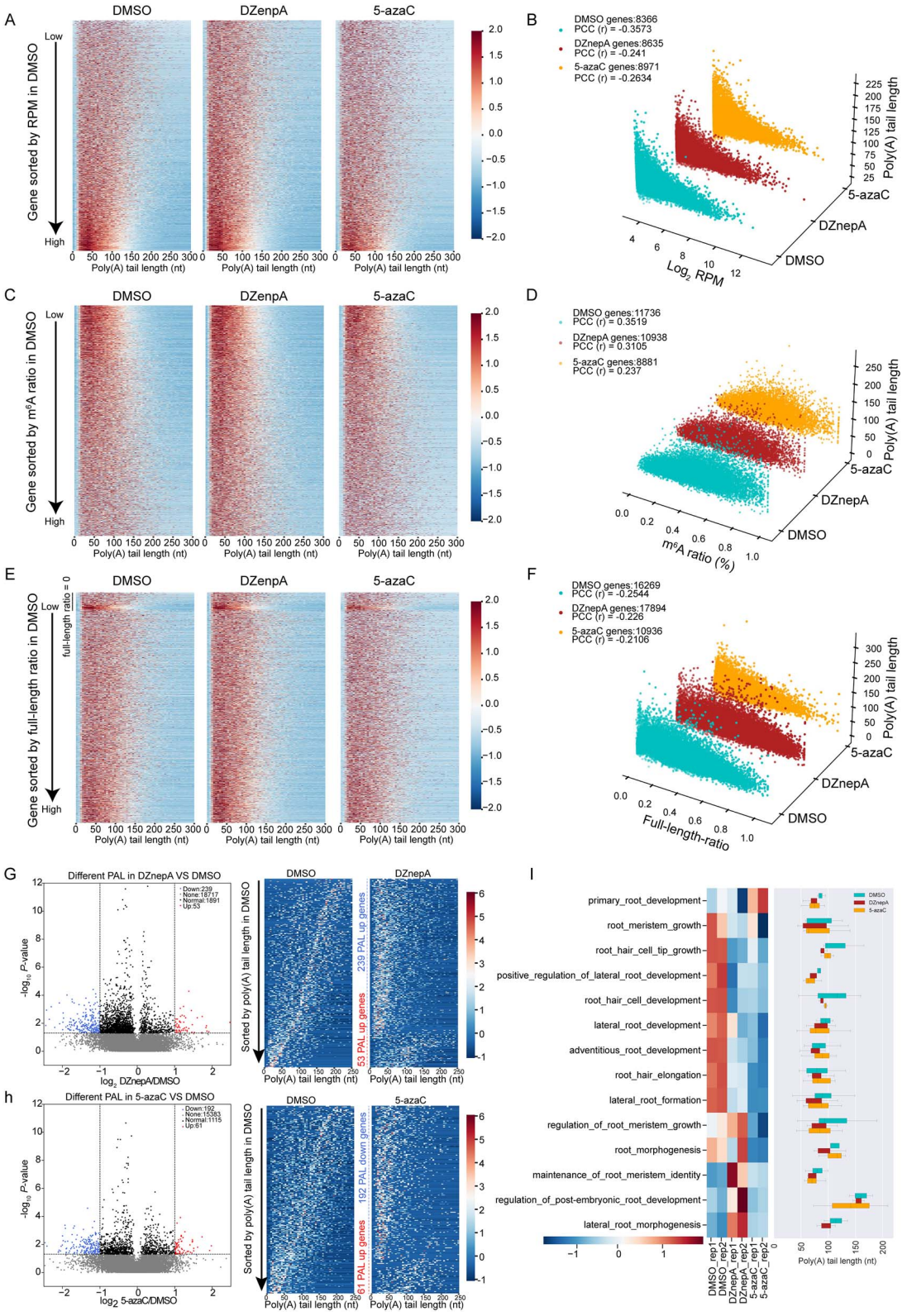

Figure 5. Dynamic of poly(A) tail length upon inhibitor treatment. (A) Heatmap showing PAL distribution in genes with reads number more than 20, which were sorted by gene expression (RPM) from DMSO treatment. (B) Scatter plot showing the correlation between PAL and gene expression (RPM). (C) Heatmap showing PAL distribution in genes sorted by m^6A ratio from DMSO treatment. (D) Scatter plot showing the correlation between gene PAL and m^6A ratio. (D) Heatmap showing PAL distribution in genes sorted by full-length ratio from DMSO treatment. (F) Scatter plot showing the correlation between full-length ratio and PAL. (G, H) Volcano plot showing differentially changed PALs upon DZnepA (G) and 5-azaC (H) treatment. (I) Gene expression and PAL distribution of GO terms related with root development.

changes on genes involved in root development. We observed genes including GO terms associated with root meristem, root cap growth, lateral root growth, adventitious root growth and formation presented down-regulation of expression (left panel in Figure 5I), which was accompanied by shortened PAL upon DZnepA treatment (right panel in Figure 5I).

Differentially expressed genes showing overlap between DNA and RNA methylators inhibitor

To explore the methylators level upon inhibitor treatment, we performed whole-genome bisulfite sequencing (WGBS) on samples with DMSO, 5-azaC and DZnepA treatment. DNA methylators profile showed that bamboo roots treated with 5-azaC presented reduced methylators levels in transcript region of coding genes and 2 kb upstream or downstream of transcript region (Figure 6A). Moreover, DZnepA treatment also presented slightly decreased levels of mCG, mCHG and mCHH (Figure 6A). Both DZnepA and 5-azaC treatment could reduce the methylators levels (mCG, mCHG and mCHH) of transposable elements (TEs) (Figure 6B).

In order to quantify gene expression upon inhibitor, we also performed strand-specific RNA-seq on samples with DMSO, 5-azaC and DZnepA treatment. In total, we identified 2995 up-regulated genes and 2609 down-regulated genes upon DZnepA treatment using cut-off of FDR < 0.05 and fold change >1.5 or <1.5 (Figure 6C; Table S9 available as Supplementary data at *Tree Physiology* Online). Gene Ontology enrichment analysis reveals that up-regulated genes in DZnepA were enriched in the glutathione metabolism pathway, cell differentiation and secondary metabolism related genes (Figure S11A available as Supplementary data at *Tree Physiology* Online). Down-regulated genes were enriched in peroxidase activity, reduction reaction, cell wall and photosynthesis related genes (Figure S11B available as Supplementary data at *Tree Physiology* Online). There were 5249 significantly changed expressed genes upon 5-azaC treatment, including 3512 up-regulated and 1737 down-regulated genes (Figure 6D; Table S10 available as Supplementary data at *Tree Physiology* Online). DNA hypomethylation was reported to enhance photosynthesis (H. Jia et al. 2022). We found that GO terms of up-regulated genes show enrichment in chloroplast thylakoid membrane and related to photosynthesis (Figure S12A available as Supplementary data at *Tree Physiology* Online). The down-regulated genes were enriched in the cell wall synthesis and peroxidase activity (Figure S12B available as Supplementary data at *Tree Physiology* Online).

To investigate the associations between m^6A and 5mC, we observed the overlapped differentially expressed genes (DEGs) upon DZnepA and 5-azaC treatment. Notably, we observed great percentage of overlap among down-regulated DEGs (Figure 6E) and up-regulated DEGs (Figure 6F) upon inhibitor treatment. The GO enrichment of overlapped DEG at down-regulated in both DZnepA and 5-azaC showed that the root growth, organization of cell wall and peroxidase activity were inhibited after DZnepA and 5-azaC treatment (Figure 6E; Figure S13A available as Supplementary data at *Tree Physiology* Online). Glutathione is a dominant endogenous antioxidant involved in H_2O_2 detoxification through different glutathione peroxidase (Skopelitis et al. 2006, Gu et al. 2015). Overlapping 1268 down-regulated genes involving peroxidase activity (Figure 6E; Figure S13A available as Supplementary data at *Tree Physiology* Online) and overlapping 1862 up-regulated including glutathione transferase activity (Figure 6F; Figure S13B available as Supplementary data at *Tree Physiology* Online) implied that moso bamboo roots might alter redox pathways in response to inhibitor toxicity. In addition, 176 overlapped-genes down-regulated in DZnepA and up-regulated in 5-azaC indicated that photosynthesis exhibited enhancement in 5-azaC and inhibition in DZnepA (Figure 6G), which may be related to the GSH-mediated imbalance of carbon and nitrogen metabolism leading to inhibition of photorespiration (Yan et al. 2021) (Figure S13C available as Supplementary data at *Tree Physiology* Online). However, there was only one overlapped-gene in up-regulated in DZnepA and down-regulated in 5-azaC (Figure 6H).

In this study, we found that m^6A level exhibited a negative relation with gene expression (Figure S14 available as Supplementary data at *Tree Physiology* Online), which was consistent with previous studies (Shen et al. 2016, Zhou et al. 2019, Gao et al. 2021). We detected 713 genes with differences in both m^6A ratio (log2 fold change $> |0.5|$) and expression (log2 fold change $> |1|$) (Figure 6I; Table S11 available as Supplementary data at *Tree Physiology* Online). We found genes with glutathione transferase activity showed lower m^6A ratio and increased expression (red scatter in Figure 6I). Additionally, we detected a total of 666 genes with differences in both m^6A modification and expression in 5-azaC-treated bamboo (Figure 6J; Table S11 available as Supplementary data at *Tree Physiology* Online). Photosynthesis-related genes were enriched in quadrant 2, demonstrating the potential relation between m^6A and expression in these genes (green scatter in Figure 6J). Notably, cell wall organization genes showed m^6A hypermethylation and low expression in both DZnepA and 5-azaC (blue scatter in Figure 6I and J). The inhibition of root growth might be caused by the changed m^6A, which were accompanied by decreased expression of cell wall organization genes.

Long non-coding RNA presented high percentage of increased expression in response to inhibitors treatment

Long non-coding RNAs (lncRNAs) have been identified based on ONT long reads in multiple species (Kirov et al. 2020, Liang et al. 2021). Based on lncRNAs identification pipeline (Figure 7A), we identified a total of 5500 high-confident lncRNAs, which presented shorter exon length than that of coding genes (Figure 7B). We found that lncRNA in this study had

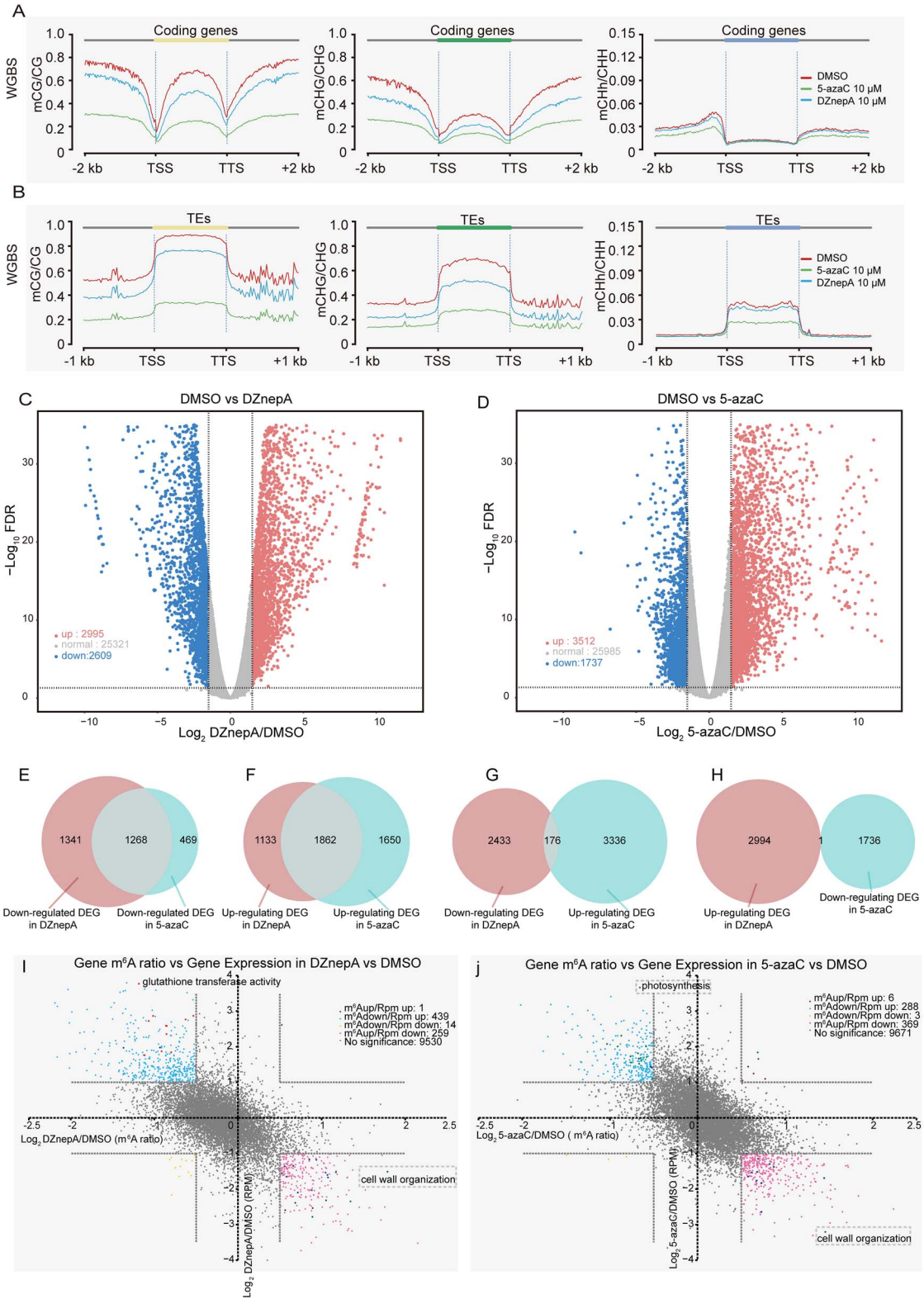

Figure 6. Global DNA methylators profile and overlapped DEGs upon two inhibitors treatment. (A) Global DNA methylators level of coding genes upon 5-azaC and DZnepA treatment. (B) DNA methylators level of TEs upon 5-azaC and DZnepA treatment. (C, D) Volcano plots showing DEGs upon DZnepA (C) and 5-azaC (D) treatment. (E–H) Venn diagram showing overlap of DEGs between DZnepA and 5-azaC. (I, J) Scatter plot showing the association between m^6A ratio and gene expression upon DZnepA (I) and 5-azaC (J) treatment.

higher percentage of full-length ratio than that of protein-coding genes (left panel in Figure 7C), which suggests that lncRNA might present a low degradation rate. However, long non-coding genes were annotated, and the full-length ratio was calculated using the same DRS libraries, which partly explained why the percentage of full-length ratio in non-coding genes was higher than that of protein-coding genes. Thus, more evidence was required to confirm the turnover rate of lncRNAs.

In total, there were 43 lncRNAs with up-regulated full-length ratios (Figure 7D) and 99 lncRNAs with down-regulated full-length ratios (Figure 7E) upon DZnepA and 5-azaC treatment, respectively. The lncRNA shared a similar m^{6}A modified ratio with that of protein-coding genes (Figure 7F). However, the enrichment m^{6}A region presented a shift towards the middle region that of noncoding genes, as compared to, as compared to the distribution observed in coding genes (Figure 7G). Furthermore, we identified 979 up-regulated lncRNAs and only 196 down-regulated lncRNAs upon DZnepA treatment (Figure 7H). The up-regulated lncRNAs presented a significantly lower m^{6}A modified ratio (Figure 7I, $P = 0.0026$). However, 5-azaC treatment did not present this trend (Figure 7I and J, $P = 0.947$). The full-length ratio did present obvious association with the up-regulation or down-regulation of these differentially expressed lncRNAs (Figure 7I and K).

The change in expression of genes regulating RNA and DNA methylation

The m^{6}A readers, writers and erasers regulate the m^{6}A epitranscriptome. In this study, we investigated the expression of 11 m^{6}A writers, 14 erasers and 26 readers based on RNA-seq (Table S12 available as Supplementary data at *Tree Physiology* Online). We found that two m^{6}A writers (*PedFIONA1* and *PedMTA*) and seven m^{6}A readers presented up-regulation upon DZnepA treatment (Figure 8A), which might counterwork to the whole hypomethylation due to inhibitors of m^{6}A. The heatmap-based tags per million (TPM) from m^{6}A regulatory gene family further revealed that m^{6}A writers such as *MTA* and *MTB* showed increased expression upon DZnepA treatment (Figure S15A available as Supplementary data at *Tree Physiology* Online). The potential m^{6}A erasers could be classified into three groups according to the expression level (Figure S15B available as Supplementary data at *Tree Physiology* Online). Group1 (*ALKBH1* and *ALKBH6*) and group2 (*ALKBH9B*) showed increased expression in response to DZnepA and 5-azaC, respectively. However, group 3 (*ALKBH10B* family) showed decreased expression upon DZnepA and 5-azaC treatment (Figure S15B available as Supplementary data at *Tree Physiology* Online). Most m^{6}A reader genes including *CPSF30* and YTHDFa family showed overall up-regulation, which were accompanied by hypo-methylated m^{6}A (PH02Gene03570, PH02Gene28571, PH02Gene14008 and PH02Gene15172) upon DZnepA treatment (Figure S15C available as Supplementary data at *Tree Physiology* Online). Among 19 m^{6}A reader genes, only three genes with YTHDFc domain decreased upon DZnepA treatment. Though we found up-regulated expression of two m^{6}A erasers and one reader upon 5-azaC treatment (Figure 8B), these genes were relatively more stable than those of DZnepA treatment.

Moreover, we also investigated the expression levels of DNA methyltransferases and demethylases. The expression of both *PedMET1* (CG methylation) and *PedCMT3* (CHG methylation) was slightly down-regulated in response to DZnepA and 5-azaC treatment (Figure 8C), which was consistent with the decreasing DNA methylators level of CG and CHG, respectively. We observed increased m^{6}A modification for *PedCMT3* upon 5-azaC treatment (Figure 8D), which might be associated with the decreased expression (Figure 8C). However, we did not identify m^{6}A modification for *PedMET1* at current DRS sequence depth (Figure 8D). *PedDRM2*, the methyltransferase responsible for CHH methylation, presented increased gene expression (Figure 8C) and decreased m^{6}A modification (Figure 8D) in response to DZnepA and 5-azaC treatment. The *ROS* family are required for active demethylation in plant (Morales-Ruiz et al. 2006, Ponferrada-Marín et al. 2010). *PedROS3* showed slightly up-regulated and down-regulated in response to DZnepA and 5-azaC, respectively. Though the expression was negatively associated with m^{6}A ratio (Figure 8D), more experimental evidence was required to reveal whether expression of *PedROS3* might be regulated by m^{6}A upon inhibitors treatment.

Discussion

Epigenetics has presented great potential for improvement in crop breeding (Gallusci et al. 2017, Yu et al. 2021). RNA modification has been proved to have essential roles in many physiological functions involving development and response to environmental stress in plants (Gao et al. 2022, Zhou et al. 2022). Studies have shown that m^{6}A hypermethylation in *PtrMTA*-overexpressing poplar appeared to enhance root development (Bodi et al. 2012, Lu et al. 2020, Zhang et al. 2022). Both *MTA* (Zhong et al. 2008) and *VIRILIZER (vir-1)* (Růžička et al. 2017) are critical for the lateral root formation. DNA methylators profile in root meristem reveals that DNA hypermethylation correlates with hypermethylation levels of transposable elements in *Arabidopsis* (Kawakatsu et al. 2016). In this study, expression of most m^{6}A writers had increased upon inhibitor treatment. For example, DZnepA-treated bamboo showed m^{6}A hypomethylation and increased expression of mostly m^{6}A writers including *PedMTA* (Figure S15A available as Supplementary data at *Tree Physiology* Online, Figure 2C). This result emphasizes the necessary role of m6A writer in root development. Therefore, future work can focus on the direct effects of m^{6}A writers on the growth of *P. edulis*, such as

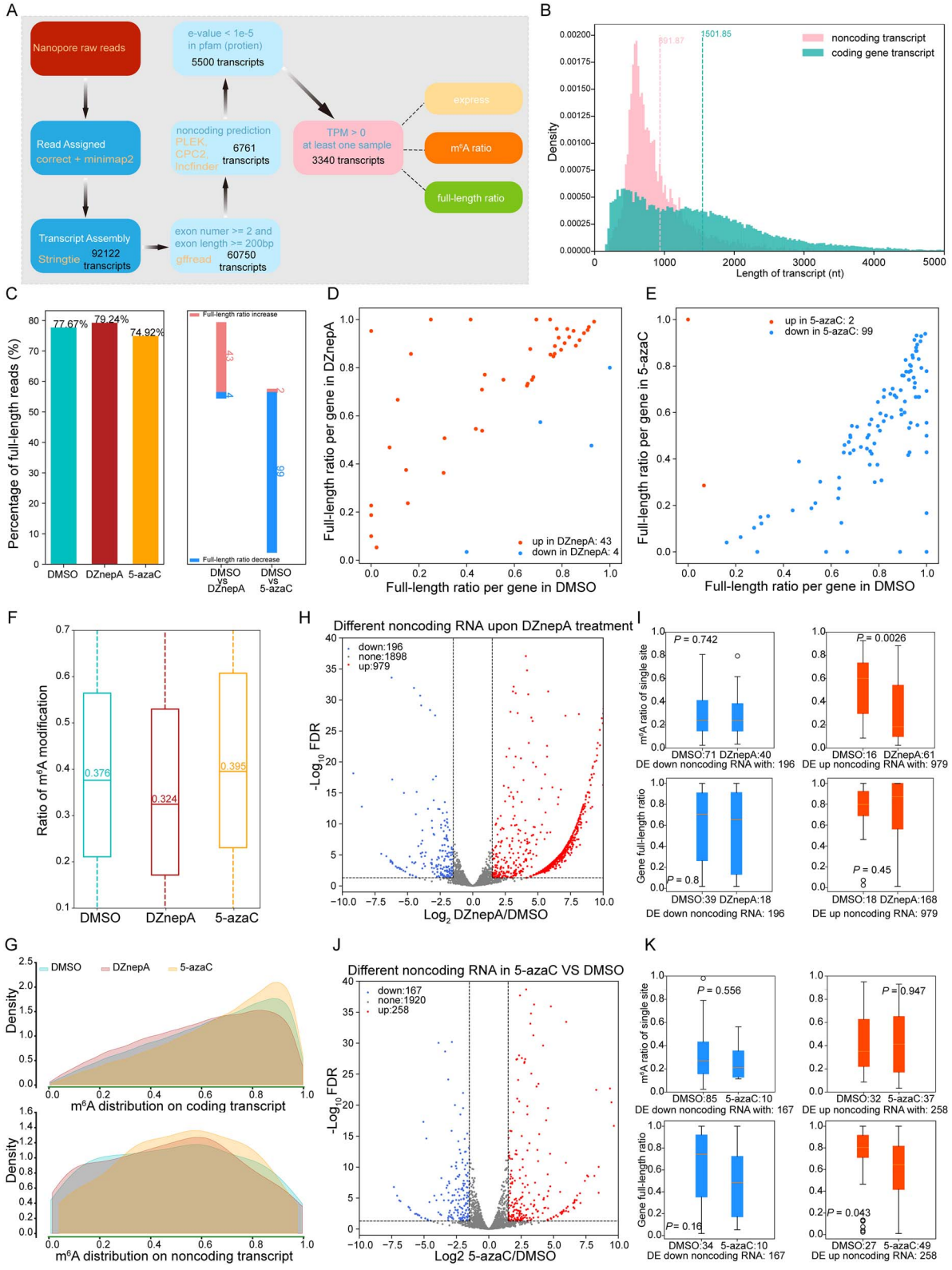

Figure 7. Identification and profile of lncRNA in root upon two inhibitors treatment. (A) The pipeline for the identification of lncRNA. (B) The density distribution of exon length from lncRNA transcripts and protein-coding transcripts. (C) Histogram in left panel showing the mean full-length ratio of lncRNA transcript in DMSO, DZnepA and 5-azaC. Histogram in right panel showing the number of lncRNAs with differential full-length ratio (Fishers' extact test, $P < 0.005$). (D, E) Scatter plot showing lncRNAs with differential full-length ratio upon DZnepA (D) and 5-azaC (E) treatment. (F) Boxplot showing m^{6}A level from lncRNA. (G) Density plot showing m^{6}A distribution in coding transcript (upper panel) and lncRNA transcript (lower panel). (H, J) Volcano plot showing differentially expressed lncRNA upon DZnepA (H) and 5-azaC (J) treatment. (I–K) Boxplot showing m^{6}A ratio and full-length ratio of differentially expressed lncRNA upon DZnepA (I) and 5-azaC (K) treatment.

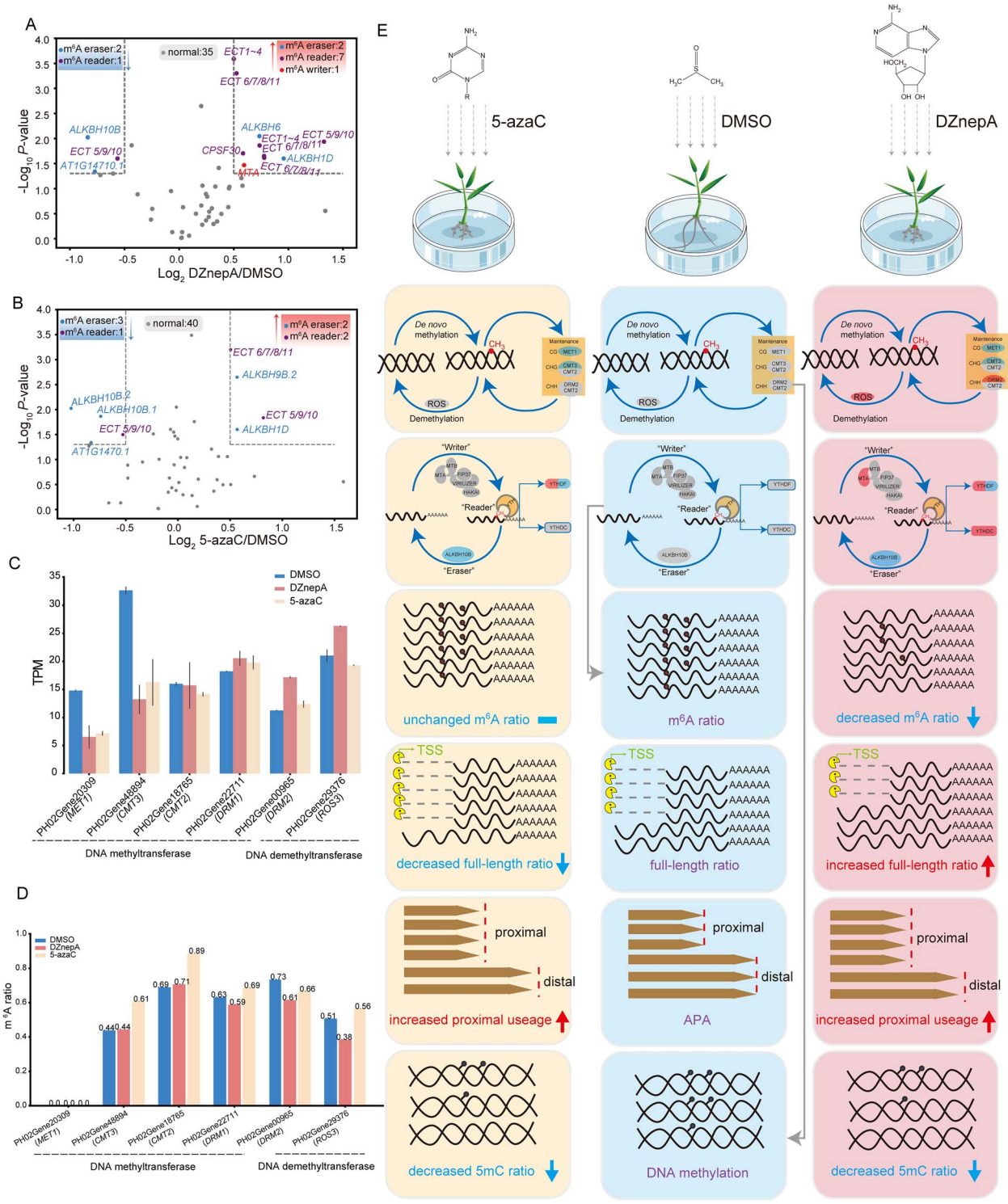

Figure 8. Dynamic change of RNA and DNA methylators regulators and models. (A, B) Scatter plot showing differentially expressed m^{6}A regulators (log2 TPM fold change > |0.5|) upon DZnepA (A) and 5-azaC (B) treatment. (C, D) Histogram showing the expression (C) and m^{6}A level (D) of DNA methyltransferase and demethyltransferase upon inhibitor treatment. (E) Regulation network of bamboo roots upon DZnepA and 5-azaC treatment.

overexpression or knockout of *PedMTA* or *PedMTB*. Additionally, the reduction of *PedALKBH10* could antagonize the m^{6}A hypomethylation in response to DZnepA treatment because the absence of *ALKBH10* could led to the global increase of m^{6}A level in *Arabidopsis* (Duan et al. 2017). The m^{6}A-mediated regulation is implemented by the m^{6}A readers including the ECT domain (Reichel et al. 2019). Readers are required for plant organogenesis during rapid cellular proliferation and exhibit

high expression in lateral root formation (Arribas-Hernández et al. 2020). We observed overall upregulation of m^{6}A readers, which might antagonize the m^{6}A hypomethylation in response to DZnepA treatment (Figure S15C available as Supplementary data at *Tree Physiology* Online). Meanwhile, the descending expression of m^{6}A readers was observed in 5-azaC-treated samples, which implied that defect of 5mC might affect the expression of m^{6}A (Figure S15C available as Supplementary data at *Tree Physiology* Online). Future work could focus on exploring how these readers and erasers interact and regulate the content of m^{6}A to provide further insights into the epitranscriptome of root development in bamboo.

In this study, we found that hypomethylated and hypermethylated m^{6}A site enriched in the 3′-UTR and CDS regions, respectively (Figure 2F). Previous study reveals that *FIONA1*, as methyltransferase, deposits m^{6}A mainly on the coding regions (Xu et al. 2022). In particular, we found the upregulated expression of *FIONA1* upon DZnepA treatment (Figure S15A available as Supplementary data at *Tree Physiology* Online). According to the result, we proposed that up-regulated *FIONA1* might be partly responsible for the deposition of m^{6}A in CDS in response to DZnepA treatment. However, pull-down experiments are required in future to validate whether *FIONA1* or other m^{6}A methyltransferases contribute to the recognition of these RNAs. Interestingly, we found that most m^{6}A regulatory proteins including writers, readers and erasers included m^{6}A modification themselves. For example, we found that *FIONA1* included m^{6}A sites (Figure S15A available as Supplementary data at *Tree Physiology* Online). Our previous studies in poplar showed that m^{6}A modification was negatively correlated with transcript abundance in response to drought stress (Gao et al. 2022). The hypomethylated m^{6}A modification of *FIONA1* could be associated with the increased expression of *FIONA1*, which might improve the whole m^{6}A modification in the coding region upon DZnepA treatment (Figure 2F). We also observed this trend in other m^{6}A regulatory proteins including ALKBH and YTHDFa/b (Figure S15 available as Supplementary data at *Tree Physiology* Online), which suggested a potential self-regulatory circuit for these RNA-binding proteins (RBPs). Exon junction complexes (EJCs) have been reported as m^{6}A suppressors to protect RNA near the exon junction from RNA methylators (He et al. 2023). In this study, we observed slightly increased expression of EJC components, such as *MAGO*, *Y14* and *EIF4A-III*, upon DZnepA treatment (Figure S16A available as Supplementary data at *Tree Physiology* Online), which might be caused due to reduced m^{6}A levels (Figure S16B available as Supplementary data at *Tree Physiology* Online).

The RNA modification has been reported to affect the full-length ratio of a downstream-specific transcript (Lee et al. 2020). In this study, we identified 2258 genes with increased full-length ratio upon DZnepA treatment (Figure 3B). We also found that full-length transcripts always presented higher m^{6}A modification than non-full-length transcripts (Figure 3E). In particular, the genes with decreased full-length ratio upon DZnepA treatment had lower m^{6}A modification (Figure 3D). The m^{6}A reader *YTHDF2* triggers mRNA degradation by deadenylation, endoribonucleolytic cleavage and decapping (Lee et al. 2020, Boo et al. 2022). Therefore, the association between RNA degradation and RNA modification might also exist in bamboo. However, more experiments are required to determine RBPs related to degradation in bamboo.

In *Arabidopsis*, 60–70% genes including APA contribute to the diversity of isoforms (Shen et al. 2011, Wu et al. 2011). Rice and poplar exhibit a shorter 3′-UTR length in response to environmental stress (Shen et al. 2011, Gao et al. 2022). Previous study indicates that mutation of an m^{6}A writer causes the conversion in poly(A) site (Xu et al. 2022). In this study, we observed proximal poly(A) shift in response to inhibitors treatment (Figure 4A and B), which was a more obvious association with DZnepA treatment. We also found the m^{6}A was more enriched in genes with the proximal transferring of APA (Figure 4C). The enrichment of m^{6}A site on the 3′-UTR might be critical for the correct formation of RNA 3′ end. Thus, mining the relationship between m^{6}A and APA on the 3′-UTR may reveal the mechanism how m^{6}A regulates diversified APA in future. It will be interesting to investigate which m^{6}A regulatory genes are associated with the APA shift in future.

Extensive studies have identified lncRNA in plants (Wang et al. 2021, Yuan et al. 2022), which are involved in transcriptional regulation and physiological function (Urquiaga et al. 2021). Although the functions of lncRNA have been explored in many plants (Bardou et al. 2014, Zhang et al. 2014, Wang et al. 2021), the relationship between m^{6}A modification and degradation on lncRNA remains unexplored in bamboo. In this study, we identified m^{6}A-enriched lncRNAs, which were different from coding genes in m^{6}A distribution (Figure 7G). We investigated the characters of exons and introns between non-coding and coding genes (Figure S17 available as Supplementary data at *Tree Physiology* Online). We discovered that m^{6}A-modified exons from non-coding genes were longer than that of coding genes (Figure S17A available as Supplementary data at *Tree Physiology* Online). Additionally, we observed longer introns (Figure S17B available as Supplementary data at *Tree Physiology* Online) and a lower number of introns (Figure S17C available as Supplementary data at *Tree Physiology* Online) for non-coding genes, which might be associated with the presence of fewer EJCs in non-coding genes and different distribution of m^{6}A between non-coding and coding genes. It is also possible those lncRNAs are recognized by distinct m^{6}A methyltransferase complex. The difference in motif distribution might also cause this divergence. In particular, we found that increased expression of lncRNAs was accompanied by decreased m^{6}A level (Figure 7H), which was consistent with that of coding genes.

Though we obtained >10 million DRS reads, the low number of long reads based on MinION sequencing was the major disadvantage compared with that of the Illumina platform. Given that low number of reads was obtained due to low depth of DRS, we speculated that m^{6}A modification would be difficult to quantify for the low-abundance genes due to lower reads coverage. Thus, we classified all m^{6}A-modified genes into two types: common modification (m^{6}A sites in both DMSO and two inhibitors treatment samples) and sample-specific modification (m^{6}A sites only in DMSO or inhibitor treatment). The genes with sample-specific modification presented lower expression than genes with common modification (Figure S18 available as Supplementary data at *Tree Physiology* Online). This result indicated that it should be careful to resolve the sample-specific modification, which might be caused by unbalanced library sizes or low sequencing depth. Unbalanced library sizes could be solved by normalization of total DRS reads. However, it was difficult to quantify the modification of genes with lower expression. Thus, we used common m^{6}A sites for the quantification analysis.

The mutual regulation between DNA methylators and RNA methylators has been reported among multiple species. During tomato fruit ripening, the transcription initiation of m^{6}A eraser (*SlALKBH2*) was mediated by DNA methylation, while the gene expression of DNA demethylase (*SlDML2*) could be regulated by m^{6}A modification (Zhou et al. 2019). In tea withering, the abundances of some m^{6}A writers show a positive correlation with those of 5mC writers. Meanwhile, several m^{6}A erasers and 5mC erasers are positively correlated (Zhu et al. 2021). Our BS-seq result demonstrated that DZnepA treatment reduced the DNA methylators level (Figure 6A and B), which could be partially explained by the down-regulation of *MET1* and *CMT3* (Figure 8C and D). Previous reports showed that 5-azaC treatment in the human cells also increases m^{6}A writer expression and exhibits a reduction of m^{6}A and 5mC (Filip et al. 2022). Although we did not find global changes of m^{6}A modification upon 5-azaC treatment (Figure 2C), we indeed observed 517 differentially expressed m^{6}A sites upon 5-azaC treatment. This observation implies potential crosstalk between 5mC and m^{6}A. However, we still need more evidences to construct the relationship network between DNA methylators and RNA methylation, which needs more research.

Conclusions

In this study, we found that the root growth was regulated by RNA methylators modification and DNA methylators in *P. edulis*. We proposed a possible model to explain the association between hypomethylation of m^{6}A and 5mC and the lateral root development of *P. edulis*. In particular, we also investigated the association of methylators and other post-transcriptional regulation, including full-length ratio, alternative polyadenylation and poly(A) tail length. This study provides preliminary association between RNA methylators and DNA methylators to promote further investigation by genetic transformation in future.

Supplementary data

Supplementary data for this article are available at *Tree Physiology* Online.

Funding

This research was funded by the National Key Research and Development Program of China (2021YFD2200505), the Natural Science Foundation of Fujian Province (2021J02027), a National Natural Science Foundation of China Grant (31971734) and the Forestry Peak Discipline Construction Project of Fujian Agriculture and Forestry University (72202200205).

Conflict of interest

The authors declare that they have no competing interests.

Authors' contributions

L.G. conceived and designed the research. Y.L., Z.Z., H.Y.W., J.Z. and H.Z. performed bioinformatics. F.X., L.W., H.H.W., B.W., W.K. and L.Z. performed experiments. L.G. and J.G. managed the project. Y.L., F.X. and L.G. wrote the manuscript.

Data availability statement

Raw sequencing data are available under accession numbers PRJNA862259 and PRJNA884826. The DRS data can be accessed on genome browser under inhibitor track at forestry.fafu.edu.cn/db/PhePacBio/phe_v2/Jbnest.php. The code used in this study is accessible at https://github.com/GulnNGS/Inhibition.

References

Arribas-Hernández L, Brodersen P (2020) Occurrence and functions of m^{6}A and other covalent modifications in plant mRNA. Plant Physiol 182:79–96.

Arribas-Hernández L, Bressendorff S, Hansen MH, Poulsen C, Erdmann S, Brodersen P (2018) An m^{6}A-YTH module controls developmental timing and morphogenesis in *Arabidopsis*. Plant Cell 30:952–967.

Arribas-Hernández L, Simonini S, Hansen MH, Botterweg Paredes E, Bressendorff S, Dong Y, Østergaard L, Brodersen P (2020) Recurrent requirement for the m^{6}A-ECT2/ECT3/ECT4 axis in the control of cell proliferation during plant organogenesis. Development 147:dev189134.

Bai F, Matton DP (2018) The *Arabidopsis* mitogen-activated protein kinase kinase kinase 20 (MKKK20) C-terminal domain interacts with MKK3 and harbors a typical DEF mammalian MAP kinase docking site. Plant Signal Behav 13:1–5.

Bardou F, Ariel F, Simpson CG, Romero-Barrios N, Laporte P, Balzergue S, Brown JWS, Crespi M (2014) Long noncoding RNA modulates alternative splicing regulators in *Arabidopsis*. Dev Cell 30:166–176.

Bartee L, Malagnac F, Bender J (2001) *Arabidopsis* cmt3 chromomethylase mutations block non-CG methylation and silencing of an endogenous gene. Genes Dev 15:1753–1758.

Bodi Z, Zhong S, Mehra S, Song J, Graham N, Li H, May S, Fray RG (2012) Adenosine methylation in *Arabidopsis* mRNA is associated with the 3′ end and reduced levels cause developmental defects. Front Plant Sci 3:48.

Boo S, Ha H, Lee Y, Shin M, Lee S, Kim Y (2022) UPF1 promotes rapid degradation of m^{6}A-containing RNAs. Cell Rep 39:110861–110875. https://doi.org/10.1016/j.celrep.2022.110861.

Bouyer D, Kramdi A, Kassam M, Heese M, Schnittger A, Roudier F, Colot V (2017) DNA methylation dynamics during early plant life. Genome Biol 18:179. https://doi.org/10.1186/s13059-017-1313-0.

Burn J, Bagnall D, Metzger J, Dennis E, Peacock W (1993) DNA methylation, vernalization, and the initiation of flowering. Proc Natl Acad Sci USA 90:287–291.

Chaowana P (2013) Bamboo: an alternative raw material for wood and wood-based composites. J Mater Sci Res 2:90.

Christman J (2002) 5-Azacytidine and 5-aza-2′-deoxycytidine as inhibitors of DNA methylation: mechanistic studies and their implications for cancer therapy. Oncogene 21:5483–5495.

Conesa A, Gotz S, Garcia-Gomez J, Terol J, Talon M, Robles M (2005) Blast2GO: a universal tool for annotation, visualization and analysis in functional genomics research. Bioinformatics 21:3674–3676.

Coots R, Liu X, Mao Y, Dong L, Zhou J, Wan J, Zhang X, Qian S (2017) m^{6}A facilitates eIF4F-independent mRNA translation. Mol Cell 68:504–514.e7.

Daccord N, Celton J-M, Linsmith G et al. (2017) High-quality *de novo* assembly of the apple genome and methylome dynamics of early fruit development. Nat Genet 49:1099–1106.

Duan H, Wei L, Zhang C, Wang Y, Chen L, Lu Z, Chen PR, He C, Jia G (2017) ALKBH10B is an RNA N^6-methyladenosine demethylase affecting *Arabidopsis* floral transition. Plant Cell 29:2995–3011.

Ebbs ML, Bender J (2006) Locus-specific control of DNA methylation by the *Arabidopsis* SUVH5 histone methyltransferase. Plant Cell 18:1166–1176.

Edens BM, Vissers C, Su J et al. (2019) FMRP modulates neural differentiation through m^{6}A-dependent mRNA nuclear export. Cell Rep 28:845–854.e5.

Filip K, Lewińska A, Adamczyk-Grochala J, Marino Gammazza A, Cappello F, Lauricella M, Wnuk M (2022) 5-Azacytidine inhibits the activation of senescence program and promotes cytotoxic autophagy during Trdmt1-mediated oxidative stress response in insulinoma β-TC-6 cells. Cell 11:1213. https://doi.org/10.3390/cells11071213.

Friedman S (1979) The effect of 5-azacytidine on *E. coli* DNA methylase. Biochem Biophys Res Commun 89:1328–1333.

Fustin J, Doi M, Yamaguchi Y et al. (2013) RNA-methylation-dependent RNA processing controls the speed of the circadian clock. Cell 155:793–806.

Gallusci P, Dai Z, Génard M, Gauffretau A, Leblanc-Fournier N, Richard-Molard C, Vile D, Brunel-Muguet S (2017) Epigenetics for plant improvement: current knowledge and modeling avenues. Trends Plant Sci 22:610–623.

Gao Y, Liu X, Wu B, Wang H, Xi F, Kohnen M, Reddy A, Gu L (2021) Quantitative profiling of N^6-methyladenosine at single-base resolution in stem-differentiating xylem of *Populus trichocarpa* using Nanopore direct RNA sequencing. Genome Biol 22:1–17.

Gao Y, Liu X, Jin Y et al. (2022) Drought induces epitranscriptome and proteome changes in stem-differentiating xylem of *Populus trichocarpa*. Plant Physiol 190:459–479.

Garalde DR, Snell EA, Jachimowicz D et al. (2018) Highly parallel direct RNA sequencing on an array of nanopores. Nat Methods 15:201–206.

Glazer R, Knode M, Tseng C, Haines D, Marquez V (1986) 3-deazaneplanocin a: a new inhibitor of S-adenosylhomocysteine synthesis and its effects in human colon carcinoma cells. Biochem Pharmacol 35:4523–4527.

Goldstrohm A, Wickens M (2008) Multifunctional deadenylase complexes diversify mRNA control. Nat Rev Mol Cell Biol 9:337–344.

Grover J, Kendall T, Baten A, Burgess D, Freeling M, King GJ, Mosher RA (2018) Maternal components of RNA-directed DNA methylation are required for seed development in *Brassica rapa*. Plant J 94:575–582.

Gu F, Chauhan V, Chauhan A (2015) Glutathione redox imbalance in brain disorders. Curr Opin Clin Nutr Metab Care 18:89–95.

Guo T, Liu C, Meng F et al. (2022) The m^6 a reader MhYTP2 regulates MdMLO19 mRNA stability and antioxidant genes translation efficiency conferring powdery mildew resistance in apple. Plant Biotechnol J 20:511–525.

Han S, Liang Y, Ma Q, Xu Y, Zhang Y, Du W, Wang C, Li Y (2019) LncFinder: an integrated platform for long non-coding RNA identification utilizing sequence intrinsic composition, structural information and physicochemical property. Brief Bioinform 20: 2009–2027.

He P, Wei J, Dou X et al. (2023) Exon architecture controls mRNA m^{6}A suppression and gene expression. Science 379:677–682.

Hossain M, Kawakatsu T, Kim K et al. (2017) Divergent cytosine DNA methylation patterns in single-cell, soybean root hairs. New Phytol 214:808–819.

Hou N, Li C, He J et al. (2022) MdMTA-mediated m^{6}A modification enhances drought tolerance by promoting mRNA stability and translation efficiency of genes involved in lignin deposition and oxidative stress. New Phytol 234:1294–1314.

Hu H, Yang W, Zheng Z, Niu Z, Yang Y, Wan D, Liu J, Ma T (2020) Analysis of alternative splicing and alternative polyadenylation in *Populus alba* var. *pyramidalis* by single-molecular long-read sequencing. Front Genet 11:48. https://doi.org/10.3389/fgene.2020.00048.

Hu J, Cai J, Umme A, Chen Y, Xu T, Kang H (2022) Unique features of mRNA m^{6}A methylomes during expansion of tomato (*Solanum lycopersicum*) fruits. Plant Physiol 188:2215–2227.

Jackson J, Johnson L, Jasencakova Z et al. (2004) Dimethylation of histone H3 lysine 9 is a critical mark for DNA methylation and gene silencing in *Arabidopsis thaliana*. Chromosoma 112: 308–315.

Jackson J, Lindroth A, Cao X, Jacobsen SE (2002) Control of CpNpG DNA methylation by the KRYPTONITE histone H3 methyltransferase. Nature 416:556–560.

Jenjaroenpun P, Wongsurawat T, Wadley T et al. (2021) Decoding the epitranscriptional landscape from native RNA sequences. Nucleic Acids Res 49:e7. https://doi.org/10.1093/nar/gkaa620.

Jia G, Fu Y, Zhao X et al. (2011) N^6-Methyladenosine in nuclear RNA is a major substrate of the obesity-associated FTO. Nat Chem Biol 7:885–887.

Jia H, Jia H, Lu S et al. (2022) DNA and histone methylation regulates different types of fruit ripening by transcriptome and proteome analyses. J Agric Food Chem 70:3541–3556.

Jia J, Lu W, Liu B et al. (2022) An atlas of plant full-length RNA reveals tissue-specific and monocots-dicots conserved regulation of poly(A) tail length. Nat Plants 8:1118–1126.

Jones L, Ratcliff F, Baulcombe DC (2001) RNA-directed transcriptional gene silencing in plants can be inherited independently of the RNA trigger and requires MET1 for maintenance. Curr Biol 11: 747–757.

Kang Y, Yang D, Kong L, Hou M, Meng Y, Wei L, Gao G (2017) CPC2: a fast and accurate coding potential calculator based on sequence intrinsic features. Nucleic Acids Res 45:W12–W16.

Kankel M, Ramsey D, Stokes T, Flowers S, Haag J, Jeddeloh J, Riddle N, Verbsky M, Richards E (2003) *Arabidopsis* MET1 cytosine methyltransferase mutants. Genetics 163:1109–1122.

Kawakatsu T, Stuart T, Valdes M et al. (2016) Unique cell-type-specific patterns of DNA methylation in the root meristem. Nat Plants 2:16058. https://doi.org/10.1038/nplants.2016.58.

Kim D, Paggi JM, Park C, Bennett C, Salzberg S (2019) Graph-based genome alignment and genotyping with HISAT2 and HISAT-genotype. Nat Biotechnol 37:907–915.

Kirov I, Dudnikov M, Merkulov P, Shingaliev A, Omarov M, Kolganova E, Sigaeva A, Karlov G, Soloviev A (2020) Nanopore RNA sequencing revealed long non-coding and LTR retrotransposon-related RNAs expressed at early stages of triticale seed development. Plan Theory 9:1794.

Kovaka S, Zimin A, Pertea G, Razaghi R, Salzberg S, Pertea M (2019) Transcriptome assembly from long-read RNA-seq alignments with StringTie2. Genome Biol 20:278.

Krauss U, Minh B, Losi A, Gärtner W, Eggert T, von Haeseler A, Jaeger K (2009) Distribution and phylogeny of light-oxygen-voltage-blue-light-signaling proteins in the three kingdoms of life. J Bacteriol 191:7234–7242.

Krueger F, Andrews S (2011) Bismark: a flexible aligner and methylation caller for Bisulfite-Seq applications. Bioinformatics 27: 1571–1572.

Kumar R, Khandelwal N, Chander Y et al. (2022) S-adenosylmethionine-dependent methyltransferase inhibitor DZNep blocks transcription and translation of SARS-CoV-2 genome with a low tendency to select for drug-resistant viral variants. Antiviral Res 197:105232. https://doi.org/10.1016/j.antiviral.2021.105232.

Kumar S, Mohapatra T (2021) Dynamics of DNA methylation and its functions in plant growth and development. Front Plant Sci 12:596236. https://doi.org/10.3389/fpls.2021.596236.

Law JA, Jacobsen SE (2010) Establishing, maintaining and modifying DNA methylation patterns in plants and animals. Nat Rev Genet 11:204–220.

Lee Y, Choe J, Park O, Kim Y (2020) Molecular mechanisms driving mRNA degradation by m^{6}A modification. Trends Genet 36: 177–188.

Li A, Zhang J, Zhou Z (2014) PLEK: a tool for predicting long non-coding RNAs and messenger RNAs based on an improved k-mer scheme. BMC Bioinformatics 15:1–10.

Li H (2018) Minimap2: pairwise alignment for nucleotide sequences. Bioinformatics 34:3094–3100.

Li H, Handsaker B, Wysoker A et al. (2009) The sequence alignment/map format and SAMtools. Bioinformatics 25:2078–2079.

Li L, Cheng Z, Ma Y, Bai Q, Li X, Cao Z, Wu Z, Gao J (2018) The association of hormone signalling genes, transcription and changes in shoot anatomy during moso bamboo growth. Plant Biotechnol J 16:72–85.

Li R, Werger M, Kroon H, During H, Zhong Z (2000) Interactions between shoot age structure, nutrient availability and physiological integration in the giant bamboo *Phyllostachys pubescens*. Plant Biol 2:437–446.

Li T, Wang H, Zhang Y et al. (2022) Comprehensive profiling of epigenetic modifications in fast-growing moso bamboo shoots. Plant Physiol 191:1017–1035.

Li Z, Wang R, Gao Y et al. (2017). The Arabidopsis CPSF30-L gene plays an essential role in nitrate signaling and regulates the nitrate transceptor gene NRT 1.1. New Phytologist 216,1205–1222.

Liang Y, Gong Z, Wang J et al. (2021) Nanopore-based comparative transcriptome analysis reveals the potential mechanism of high-temperature tolerance in cotton (*Gossypium hirsutum* L.). Plan Theory 10:2517. https://doi.org/10.3390/plants10112517.

Liao Y, Smyth G, Shi W (2014) featureCounts: an efficient general purpose program for assigning sequence reads to genomic features. Bioinformatics 30:923–930.

Lima S, Chipman L, Nicholson A, Chen Y, Yee B, Yeo G, Coller J, Pasquinelli A (2017) Short poly(A) tails are a conserved feature of highly expressed genes. Nat Struct Mol Biol 24:1057–1063.

Liu H, Begik O, Lucas M et al. (2019) Accurate detection of m^{6}A RNA modifications in native RNA sequences. Nat Commun 10:4079.

Liu J, Yue Y, Han D et al. (2014) A METTL3-METTL14 complex mediates mammalian nuclear RNA N^6-adenosine methylation. Nat Chem Biol 10:93–95.

Liufu Y, Liu X, Wu L, Zhang H, Gao Y, Gu L (2022) An analysis pipeline for identification of RNA modification, alternative splicing and polyadenylation using third generation sequencing. Bio Protoc 12:e4433.

Lu L, Zhang Y, He Q, Qi Z, Zhang G, Xu W, Yi T, Wu G, Li R (2020) MTA, an RNA m^{6}A methyltransferase, enhances drought tolerance by regulating the development of trichomes and roots in poplar. Int J Mol Sci 21:2462. https://doi.org/10.3390/ijms21072462.

Luo G, MacQueen A, Zheng G et al. (2014) Unique features of the m^{6}A methylome in *Arabidopsis thaliana*. Nat Commun 5:5630. https://doi.org/10.1038/ncomms6630.

Ma K, Han J, Zhang Z, Li H, Zhao Y, Zhu Q, Xie Y, Liu Y, Chen L (2021) OsEDM2L mediates m^{6}A of EAT1 transcript for proper alternative splicing and polyadenylation regulating rice tapetal degradation. J Integr Plant Biol 63:1982–1994.

MacDonald C (2019) Tissue-specific mechanisms of alternative polyadenylation: testis, brain, and beyond (2018 update). WIREs RNA 10:e1526. https://doi.org/10.1002/wrna.1526.

Malagnac F, Bartee L, Bender J (2002) An Arabidopsis SET domain protein required for maintenance but not establishment of DNA methylation. EMBO J 21:6842–6852.

Miao Z, Zhang T, Qi Y, Song J, Han Z, Ma C (2020) Evolution of the RNA N^6-methyladenosine methylome mediated by genomic duplication. Plant Physiol 182:345–360.

Mistry J, Chuguransky S, Williams L et al. (2021) Pfam: the protein families database in 2021. Nucleic Acids Res 49:D412–D419.

Morales-Ruiz T, Ortega-Galisteo A, Ponferrada-Marín M, Martínez-Macías M, Ariza R, Roldán-Arjona T (2006) DEMETER and REPRESSOR OF SILENCING 1 encode 5-methylcytosine DNA glycosylases. Proc Natl Acad Sci USA 103:6853–6858.

Naumann U, Daxinger L, Kanno T, Eun C, Long Q, Lorkovic Z, Matzke M, Matzke A (2011) Genetic evidence that DNA methyltransferase DRM2 has a direct catalytic role in RNA-directed DNA methylation in *Arabidopsis thaliana*. Genetics 187:977–979.

Nicholson A, Pasquinelli A (2019) Tales of detailed poly(A) tails. Trends Cell Biol 29:191–200.

Ortega-Galisteo A, Morales-Ruiz T, Ariza R, Roldán-Arjona T (2008) *Arabidopsis* DEMETER-LIKE proteins DML2 and DML3 are required for appropriate distribution of DNA methylation marks. Plant Mol Biol 67:671–681.

Parker M, Knop K, Sherwood A, Schurch N, Mackinnon K, Gould P, Hall A, Barton G, Simpson G (2020) Nanopore direct RNA sequencing maps the complexity of *Arabidopsis* mRNA processing and m^{6}A modification. Elife 9:e49658.

Passmore LA, Coller J (2022) Roles of mRNA poly(A) tails in regulation of eukaryotic gene expression. Nat Rev Mol Cell Biol 23:93–106.

Peng Z, Lu Y, Li L et al. (2013) The draft genome of the fast-growing non-timber forest species moso bamboo (*Phyllostachys heterocycla*). Nat Genet 45:456–461.

Penterman J, Zilberman D, Huh J, Ballinger T, Henikoff S, Fischer R (2007) DNA demethylation in the *Arabidopsis* genome. Proc Natl Acad Sci USA 104:6752–6757.

Plongthongkum N, Diep D, Zhang K (2014) Advances in the profiling of DNA modifications: cytosine methylation and beyond. Nat Rev Genet 15:647–661.

Ponferrada-Marín M, Martínez-Macías M, Morales-Ruiz T, Roldán-Arjona T, Ariza R (2010) Methylation-independent DNA binding modulates specificity of repressor of silencing 1 (ROS1) and facilitates demethylation in long substrates. J Biol Chem 285:23032–23039.

Pontier D, Picart C, El Baidouri M et al. (2019) The m^{6}A pathway protects the transcriptome integrity by restricting RNA chimera formation in plants. Life Sci Alliance 2:e201900393. https://doi.org/10.26508/lsa.201900393.

Qi X, Wu Z, Li J, Mo X, Wu S, Chu J, Wu P (2007) AtCYT-INV1, a neutral invertase, is involved in osmotic stress-induced inhibition on lateral root growth in *Arabidopsis*. Plant Mol Biol 64:575–587.

Rand A, Jain M, Eizenga J, Musselman-Brown A, Olsen H, Akeson M, Paten B (2017) Mapping DNA methylation with high-throughput nanopore sequencing. Nat Methods 14:411–413.

Rapp RA, Wendel JF (2005) Epigenetics and plant evolution. New Phytol 168:81–91.

Reichel M, Köster T, Staiger D (2019) Marking RNA: m^{6}A writers, readers, and functions in *Arabidopsis*. J Mol Cell Biol 11:899–910.

Roach N, Sadowski N, Alessi AF, Timp W, Taylor J, Kim J (2020) The full-length transcriptome of *C. elegans* using direct RNA sequencing. Genome Res 30:299–312.

Robinson M, McCarthy D, Smyth G (2010) edgeR: a Bioconductor package for differential expression analysis of digital gene expression data. Bioinformatics 26:139–140.

Roundtree I, Luo G, Zhang Z et al. (2017) YTHDC1 mediates nuclear export of N^6-methyladenosine methylated mRNAs. Elife 6:e31311. https://doi.org/10.7554/eLife.31311.

Růžička K, Zhang M, Campilho A et al. (2017) Identification of factors required for m^{6}A mRNA methylation in *Arabidopsis* reveals a role for the conserved E3 ubiquitin ligase HAKAI. New Phytol 215:157–172.

Salmela L, Rivals E (2014) LoRDEC: accurate and efficient long read error correction. Bioinformatics 30:3506–3514.

Schoft V, Chumak N, Choi Y et al. (2011) Function of the DEMETER DNA glycosylase in the *Arabidopsis thaliana* male gametophyte. Proc Natl Acad Sci USA 108:8042–8047.

Shemer O, Landau U, Candela H, Zemach A, Eshed WL (2015) Competency for shoot regeneration from *Arabidopsis* root explants is regulated by DNA methylation. Plant Sci 238:251–261.

Shen L, Liang Z, Gu X et al. (2016) N^6-methyladenosine RNA modification regulates shoot stem cell fate in *Arabidopsis*. Dev Cell 38:186–200.

Shen Y, Venu R, Nobuta K et al. (2011) Transcriptome dynamics through alternative polyadenylation in developmental and environmental responses in plants revealed by deep sequencing. Genome Res 21:1478–1486.

Simpson J, Workman R, Zuzarte P, David M, Dursi L, Timp W (2017) Detecting DNA cytosine methylation using nanopore sequencing. Nat Methods 14:407–410.

Skopelitis D, Paranychianakis N, Paschalidis K et al. (2006) Abiotic stress generates ROS that signal expression of anionic glutamate dehydrogenases to form glutamate for proline synthesis in tobacco and grapevine. Plant Cell 18:2767–2781.

Smith A, Jain M, Mulroney L, Garalde D, Akeson M (2019) Reading canonical and modified nucleobases in 16S ribosomal RNA using nanopore native RNA sequencing. PloS One 14:e0216709.

Song P, Yang J, Wang C, Lu Q, Shi L, Tayier S, Jia G (2021) *Arabidopsis* N^6-methyladenosine reader CPSF30-L recognizes FUE signals to control polyadenylation site choice in liquid-like nuclear bodies. Mol Plant 14:571–587.

Song X, Peng C, Zhou G, Gu H, Li Q, Zhang C (2016) Dynamic allocation and transfer of non-structural carbohydrates, a possible mechanism for the explosive growth of Moso bamboo (*Phyllostachys heterocycla*). Sci Rep 6:25908.

Stoiber M, Quick J, Egan R, Eun Lee J, Celniker S, Neely R, Loman N, Pennacchio L, Brown J (2017) *De novo* identification of DNA modifications enabled by genome-guided Nanopore signal processing. bioRxiv 094672; not peer reviewed. https://github.com/nanoporetech/tombo.

Stroud H, Do T, Du J, Zhong X, Feng S, Johnson L, Patel D, Jacobsen S (2014) Non-CG methylation patterns shape the epigenetic landscape in *Arabidopsis*. Nat Struct Mol Biol 21:64–72.

Theler D, Dominguez C, Blatter M, Boudet J, Allain F (2014) Solution structure of the YTH domain in complex with N^6-methyladenosine RNA: a reader of methylated RNA. Nucleic Acids Res 42:13911–13919.

Thomas P, Wu X, Liu M, Gaffney B, Ji G, Li Q, Hunt A (2012) Genome-wide control of polyadenylation site choice by CPSF30 in *Arabidopsis*. Plant Cell 24:4376–4388.

Urquiaga M, Thiebaut F, Hemerly A, Ferreira P (2021) From trash to luxury: the potential role of plant lncRNA in DNA methylation during abiotic stress. Front Plant Sci 11:603246.

Viegas I, de Macedo J, Serra L et al. (2022) N^6-methyladenosine in poly(A) tails stabilize VSG transcripts. Nature 604:362–370.

Wang J, Hou Y, Wang Y, Zhao H (2021) Integrative lncRNA landscape reveals lncRNA-coding gene networks in the secondary cell wall biosynthesis pathway of moso bamboo (*Phyllostachys edulis*). BMC Genomics 22:638.

Wang X, Lu Z, Gomez A et al. (2014) N^6-methyladenosine-dependent regulation of messenger RNA stability. Nature 505:117–120.

Wang X, Wu F, Xie Q et al. (2012) SKIP is a component of the spliceosome linking alternative splicing and the circadian clock in *Arabidopsis*. Plant Cell 24:3278–3295.

Wei L, Song P, Wang Y et al. (2018) The m6 a reader ECT2 controls trichome morphology by affecting mRNA stability in *Arabidopsis*. Plant Cell 30:968–985.

Wiener D, Schwartz S (2021) The epitranscriptome beyond m^{6}A. Nat Rev Genet 22:119–131.

Workman R, Tang A, Tang P et al. (2019) Nanopore native RNA sequencing of a human poly(A) transcriptome. Nat Methods 16:1297–1305.

Wu S, Zhang Y, Yao L, Wang J, Lu F, Liu Y (2022) m^{6}A-modified RNA possess distinct poly(A) tails. J Genet Genomics 50: 208–211.

Wu X, Liu M, Downie B, Liang C, Ji G, Li Q, Hunt A (2011) Genome-wide landscape of polyadenylation in Arabidopsis provides evidence for extensive alternative polyadenylation. Proc Natl Acad Sci USA 108:12533–12538.

Xiang L, Le Roy K, Bolouri-Moghaddam M, Vanhaecke M, Lammens W, Rolland F, Van den Ende W (2011) Exploring the neutral invertase–oxidative stress defence connection in *Arabidopsis thaliana*. J Exp Bot 62:3849–3862.

Xiao W, Adhikari S, Dahal U et al. (2016) Nuclear m^{6}A reader YTHDC1 regulates mRNA splicing. Mol Cell 61:507–519.

Xu T, Wu X, Wong C, Fan S, Zhang Y, Zhang S, Liang Z, Yu H, Shen L (2022) FIONA1-mediated m^{6}A modification regulates the floral transition in *Arabidopsis*. Adv Sci 9: 2103628.

Yan L, Gong Y, Luo Q et al. (2021) Heterologous expression of fungal AcGDH alleviates ammonium toxicity and suppresses photorespiration, thereby improving drought tolerance in rice. Plant Sci 305:110769. https://doi.org/10.1016/j.plantsci.2020.110769.

Yang B, Lee M, Lin M, Chang W (2022) 5-Azacytidine increases tanshinone production in salvia miltiorrhiza hairy roots through epigenetic modulation. Sci Rep 12:9349. https://doi.org/10.1038/s41598-022-12577-8.

Yu G, Wang HY, He Q (2012) clusterProfiler: an R package for comparing biological themes among gene clusters. OMICS 16: 284–287.

Yu Q, Liu S, Yu L et al. (2021) RNA demethylation increases the yield and biomass of rice and potato plants in field trials. Nat Biotechnol 39:1581–1588.

Yuan T, Zhu C, Li G, Liu Y, Yang K, Li Z, Song X, Gao Z (2022) An integrated regulatory network of mRNAs, microRNAs, and lncRNAs involved in nitrogen metabolism of moso bamboo. Front Genet 13:854346.

Yue Y, Liu J, Cui X et al. (2018) VIRMA mediates preferential m^6A mRNA methylation in 3′-UTR and near stop codon and associates with alternative polyadenylation. Cell Discov 4:10. https://doi.org/10.1038/s41421-018-0019-0.

Zhang H, Lang Z, Zhu J (2018) Dynamics and function of DNA methylation in plants. Nat Rev Mol Cell Biol 19:489–506.

Zhang M, Bodi Z, Mackinnon K, Zhong S, Archer N, Mongan N, Simpson G, Fray R (2022) Two zinc finger proteins with functions in m^6A writing interact with HAKAI. Nat Commun 13:1127.

Zhang Y, Liao J, Li YY, Zhang J, Li Q, Qu L, Shu W, Chen Y (2014) Genome-wide screening and functional analysis identify a large number of long noncoding RNAs involved in the sexual reproduction of rice. Genome Biol 15:512.

Zhao H, Peng Z, Fei B, Li L, Hu T, Gao Z, Jiang Z (2014) BambooGDB: a bamboo genome database with functional annotation and an analysis platform. Database 2014:bau006–bau006.

Zhao H, Gao Z, Wang L et al. (2018) Chromosome-level reference genome and alternative splicing atlas of moso bamboo (*Phyllostachys edulis*). GigaScience 7:giy115.

Zheng G, Dahl J, Niu Y et al. (2013) ALKBH5 is a mammalian RNA demethylase that impacts RNA metabolism and mouse fertility. Mol Cell 49:18–29.

Zhong L, Xu Y, Wang J (2010) The effect of 5-azacytidine on wheat seedlings responses to NaCl stress. Biol Plant 54:753–756.

Zhong S, Li H, Bodi Z, Button J, Vespa L, Herzog M, Fray R (2008) MTA is an *Arabidopsis* messenger RNA adenosine methylase and interacts with a homolog of a sex-specific splicing factor. Plant Cell 20:1278–1288.

Zhong S, Fei Z, Chen Y et al. (2013) Single-base resolution methylomes of tomato fruit development reveal epigenome modifications associated with ripening. Nat Biotechnol 31:154–159.

Zhong X, Yu J, Frazier K et al. (2018) Circadian clock regulation of hepatic lipid metabolism by modulation of m^6A mRNA methylation. Cell Rep 25:1816–1828.e4.

Zhou L, Tian S, Qin G (2019) RNA methylomes reveal the m^6A-mediated regulation of DNA demethylase gene SlDML2 in tomato fruit ripening. Genome Biol 20:156. https://doi.org/10.1186/s13059-019-1771-7.

Zhou L, Gao G, Tang R, Wang W, Wang Y, Tian S, Qin G (2022) m^6A-mediated regulation of crop development and stress responses. Plant Biotechnol J 20:1447–1455.

Zhu C, Zhang S, Zhou C et al. (2021) Genome-wide investigation of N^6-methyladenosine regulatory genes and their roles in tea (*Camellia sinensis*) leaves during withering process. Front Plant Sci 12:702303. https://doi.org/10.3389/fpls.2021.702303.

Zhu J, Kapoor A, Sridhar V, Agius F, Zhu J (2007) The DNA glycosylase/lyase ROS1 functions in pruning DNA methylation patterns in *Arabidopsis*. Curr Biol 17:54–59.